Cosmology: From Theory to Data

Ruth Durrer, University of Geneva

Contents:

The Cosmic Microwave Background (CMB):

- **Photon propagation in a perturbed Friedman Universe**
- **CMB temperature anisotropies & polarization**
- **Cosmological parameters from CMB observations**

Cosmological Large Scale Structure:

- **Weak lensing**
- **The perturbed luminosity distance**
- **Number counts:**
  - **redshift space distortions**
  - **lensing**
  - **large scale relativistic effects**
- **Intensity mapping**

Introduction

In the previous courses who have learned how inflation or another phase of rapid expansion or contraction can amplify quantum fluctuations and convert then into curvature fluctuations at late times. In the simplest cases these are described by the power spectrum of the curvature fluctuation ζ. In this course we study the observational signature of such fluctuations in mainly two observables: the cosmic microwave background (CMB) and large scale structure (LSS), i.e. the matter distribution in the Universe. We shall study the observable fluctuations of the radiation and matter density, the velocity and of the metric in a Friedmann Universe at first order in perturbation theory. We assume that deviations from a homogeneous and isotropic background are small and can be expanded to first order. We also assume that the statistical properties of these fluctuations are homogeneous and isotropic, i.e. there is no preferred place and no preferred direction in the Universe.

In cosmology, we cannot calculate the curvature or density fluctuation at every point position etc., we can only calculate statistical quantities (like in statistical mechanics where we do not calculate the position of each molecule or the state of each spin). We calculate so called N-point functions, e.g. of the density, $\langle\rho(\mathbf{x},t)\rangle = \rho(t)$, $\langle\rho(\mathbf{x},t)\rho(\mathbf{y},t')\rangle = \xi(|\mathbf{x}-\mathbf{y}|,t,t')$ etc. We often also consider the Fourier transform of the 2-point, 3-point etc. functions, the power spectrum, bi-spectrum etc.

$$P_\zeta(k,t,t') = \int d^3r e^{i\mathbf{kr}}\xi_\zeta(\mathbf{r},t,t')\,, \tag{1}$$

$$\langle\zeta(\mathbf{k},t)\zeta(\mathbf{k}',t')\rangle = (2\pi)^3\delta(\mathbf{k}-\mathbf{k}')P_\zeta(k,t,t')\,, \tag{2}$$

$$P_\zeta(k,t,t') = T(t,k)T(t',k)P_\zeta(k,t_0), \qquad P_\zeta(k,t_{\rm in}) \equiv P_\zeta(k)\,. \tag{3}$$

Since we consider here linear perturbations with initial conditions laid down by one single degree of freedom in the early Universe, and since their statistical properties are independent of position we can derive a set of ordinary differential equations in Fourier space. Their solution relates the initial fluctuation e.g. of the curvature, $\zeta(\mathbf{k},t_{\rm in})$, to its final value, or vice versa,

$$X(\mathbf{k},t) = T_X(k,t)\zeta(\mathbf{k},t_{\rm in})\,, \qquad P_X(k,t) = |T_X(k,t)|^2 P_\zeta(k)\,. \tag{4}$$

Here T_X is the transfer function of the perturbation variable X and it depends only on the cosmological background evolution. This is the main reason why

the observation of cosmological perturbations allows us to infer cosmological parameters: For a given background Friedman-Lemaître (FL) Universe, the functions T_X are fixed. If we know the initial conditions or rather can parametrize P_ζ in terms of a few unknown parameters, by measuring many power spectra $P_X(k,t)$, we can measure these together with the cosmological parameters. It is clear, that the inferred cosmological parameters will depend on our assumptions of $P_\zeta(k)$ and vice versa. For this reason we call this very powerful method to infer cosmological parameters always 'parameter estimation' and not 'measurement': it is always model dependent.

In the past this method has mainly been applied to the CMB and has led to the best cosmological parameter values we have with errors on the 1% level or less [1]. This comes from the fact that we have excellent CMB observations and we understand the CMB very well. Its fluctuations are small and can be treated within linear perturbation theory to reasonably good accuracy with one exception: lensing by foreground structures. But also this effect can be taken into account in a straight forward way. The discussion of the CMB is the topic of the first chapter, today.

In the second chapter we shall address the observation of cosmological large scale structure, the distribution of galaxies. In cosmology there comes an additional difficulty: All observations are on our background lightcone. The power spectrum in k-space is not an observable since it requires and integral over all of space. For small galaxy surveys this subtlety is not very important, but for the large scale surveys currently under way and planned for the next decade, this is very important.

In this course we want to study the truly observable statistical quantities on the lightcone. Here we restrict our discussion to 2-point quantities, i.e. correlation functions and power spectra. The generalisation to higher order statistics is relatively straight forward.

We shall work mainly with scalar perturbations in longitudinal gauge and use a spatially flat geometry for simplicity,

$$ds^2 = a^2(t)\left[-(1+2\Psi(\mathbf{x},t))dt^2 + (1-2\Phi(\mathbf{x},t))\delta_{ij}dx^i dx^j\right] . \qquad (5)$$

Here t denotes conformal time and $\mathcal{H} = \dot{a}/a$ is the conformal Hubble parameter. This physical Hubble parameter is $H = \mathcal{H}/a = \dot{a}/a^2$.

In a nearly Newtonian situation and a in matter dominated Universe, $\Psi = \Phi = \frac{3}{5}\zeta$. On small scales, $k \gg \mathcal{H}$, Ψ is then simply the Newtonian potential of the matter density fluctuations.

Chapter 1

The CMB

1.1 Introduction

The cosmic microwave background radiation we emitted when the temperature of the Universe was about $T_{\rm dec} \simeq 3000$K. At this temperature there were too few photons with energies higher than 1Ry and the proton electron plasma combined into neutron hydrogen, a precess called 'recombination'. The fluctuations present in the geometry, in the radiation density and in the velocity of the electrons that last scattered these photons lead to small fluctuations in the photon temperature. In this lecture we first compute these temperature fluctuations by assuming that the observed CMB photons have been emitted from a surface of constant temperature. We then briefly outline how the process of decoupling at the last scattering surface has to be taken into account and how it leads not only to temperature anisotropies but also to polarisation and we define the CMB power spectra. Finally we discuss the dependence of the spectra on cosmological parameters.

Much more details can be found in my book on the subject [2], which is however outdated in what concerns the observational aspects (A new version is under way.).

1.2 Photon Propagations in a perturbed Friedman Universe

We consider a perturbed Friedmann Universe at relatively late time, when photons have decoupled from the baryonic fluid (i.e. after recombination) and move on light-like geodesic in the perturbed geometry.

An unperturbed photon trajectory in conformal coordinates ($K = 0$),

$$d\tilde{s}^2 = a^2(-dt^2 + \delta_{ij}dx^i dx^j)$$

follows

$$(x^\mu(t)) \equiv (t, (t-t_0)\mathbf{n} + \mathbf{x}_0)\,,$$

where $\mathbf{x}_0$ is the photon position at time t_0 and $\mathbf{n}$ is the (parallel transported) photon direction. As we consider a flat Friedmann Universe ($K = 0$), the direction $\mathbf{n}$ is time independent and $\mathbf{n}^2 = \sum_{ij}\delta_{ij}n^i n^j = 1$.

The perturbed metric is of the form

$$d\tilde{s}^2 = a^2 ds^2\,, \quad \text{with} \tag{1.1}$$
$$ds^2 = (\eta_{\mu\nu} + h_{\mu\nu})\,dx^\mu\,dx^\nu, \quad \eta_{00} = -1,\ \eta_{i0} = 0,\ \eta_{ij} = \delta_{ij}\,. \tag{1.2}$$

We make use of the fact that light-like geodesics are conformally invariant. More precisely, ds^2 and $d\tilde{s}^2$ have the same light-like geodesics, only the corresponding affine parameters are different. Let us denote the two affine parameters by λ and $\tilde{\lambda}$ respectively, and the tangent vectors to the geodesic by

$$n = \frac{dx}{d\lambda}\,, \quad \tilde{n} = \frac{dx}{d\tilde{\lambda}}\,, \quad n^2 = \tilde{n}^2 = 0\,. \tag{1.3}$$

For the unperturbed geodesic $n^0 = 1$ and $\mathbf{n}^2 = 1$.
The photon 4-momentum k^μ is given by $k^\mu = \omega n^\mu$, where ω is the constant energy of the photon moving in the flat background metric. We define ω in this way such that all the perturbations are in the photon 4-velocity vector n. In an expanding universe the photon momentum is redshifted. Actually (see ex. 1), the components behave like $\tilde{n}^i \propto 1/a^2$ so that $\tilde{\mathbf{n}}^2 = a^2\sum_i(\tilde{n}^i)^2 \propto 1/a^2$, hence we have to choose $\tilde{\lambda} = a^2\lambda$. As always for light-like geodesics, $\tilde{\lambda}$ and λ are only determined up to a multiplicative constant which we have fixed by the conditions $\mathbf{n}^2 = 1$ and $\tilde{\lambda} = a^2\lambda$.

Let us now introduce perturbations. We set $n^0 = 1+\delta n^0$ and $n^i = \bar{n}^i + \delta n^i$, where $\bar{\mathbf{n}}$ denotes the unperturbed photon direction. The geodesic equation for the perturbed metric

$$ds^2 = (\eta_{\mu\nu} + h_{\mu\nu})\,dx^\mu\,dx^\nu\,, \tag{1.4}$$

yields, to first order,

$$\frac{d}{d\lambda}\delta n^\mu = -\delta\Gamma^\mu_{\alpha\beta}\bar{n}^\alpha\bar{n}^\beta\,. \tag{1.5}$$

For the energy shift (redshift), we have to determine δn^0. Since $g^{\alpha\mu} = -\eta^{\alpha\mu} +$ first order, we obtain $\delta\Gamma^0_{\alpha\beta} = -\frac{1}{2}(h_{\alpha0,\beta} + h_{\beta0,\alpha} - \dot{h}_{\alpha\beta})$, so that

$$\frac{d}{d\lambda}\delta n^0 = h_{\alpha0,\beta}n^\beta n^\alpha - \frac{1}{2}\dot{h}_{\alpha\beta}n^\alpha n^\beta\,. \tag{1.6}$$

(On the right hand side n^μ can actually be replaced by $\bar{n}^\mu$ since $h_{\alpha\beta}$ is already first order and we neglect second order terms. For notational simplicity we shall however not always write $\bar{n}^\mu$.) Integrating this equation we use $h_{\alpha0,\beta}n^\beta n^\alpha = \frac{d}{d\lambda}(h_{\alpha0}n^\alpha)$, so that the change of n^0 between some initial time t_i and some final time t_f is given by

$$\delta n^0|_i^f = \left[h_{00} + h_{0j}n^j\right]_i^f - \frac{1}{2}\int_i^f \dot{h}_{\mu\nu}n^\mu n^\nu d\lambda\,. \tag{1.7}$$

The energy of a photon with 4-momentum $\tilde{k}^\mu$ as seen by an observer moving with 4-velocity $\tilde{u}$ is given by $E = -(\tilde{u}\tilde{\cdot}\tilde{k})$. Hence, the ratio of the energy of a photon measured by some observer at t_f to the energy emitted at t_i is

$$\frac{E_f}{E_i} = \frac{(\tilde{n}\tilde{\cdot}\tilde{u})_f}{(\tilde{n}\tilde{\cdot}\tilde{u})_i} = \frac{a_i}{a_f}\frac{(n\cdot u)_f}{(n\cdot u)_i}\,, \tag{1.8}$$

where here $\tilde{\cdot}$ denotes the scalar product in an expanding universe, containing the factor a^2 and $\tilde{u}$ is the emitter and receiver 4-velocity in an expanding universe, $\tilde{u} = a^{-1}u$, while u_f and u_i are the 4-velocities of the observer and emitter respectively in the non-expanding conformally related geometry given by

$$u = (1 + h_{00}/2)\partial_t + v^i\partial_i = a\tilde{u}\,. \tag{1.9}$$

Together with $\tilde{n} = a^{-2}n$ this implies the result (1.8). The ratio a_i/a_f is the usual (unperturbed) redshift which relates $n\cdot u$ and $\tilde{n}\tilde{\cdot}\tilde{u}$ in the unperturbed universe.

We now consider scalar perturbations in longitudinal gauge. In this gauge $h_{00} = -2\Psi$, $h_{i0} = 0$ and $h_{\mu\nu}n^\mu n^\nu = -2(\dot\Psi + \dot\Phi)$. The first order geodesic perturbations then are

$$\delta n^0\big|_i^f = -2\Psi\big|_i^f + \int_i^f (\dot\Psi + \dot\Phi)\, d\lambda\,, \tag{1.10}$$

$$\delta n^j\big|_i^f = 2n^j\Phi\big|_i^f - \int_i^f \partial^j(\Psi + \Phi)\, d\lambda\,. \tag{1.11}$$

Setting $v^i = V^i$ in longitudinal gauge we obtain

$$\frac{E_f}{E_i} = \frac{1}{1+\bar z}\left(1 - \frac{\delta z}{1+\bar z}\right) \tag{1.12}$$

$$\frac{\delta z}{1+\bar z} = \left[V_j^{(b)}n^j + \Psi\right]_i^f - \int_i^f (\dot\Psi + \dot\Phi)\, d\lambda\,. \tag{1.13}$$

This is the redshift perturbation on longitudinal gauge. Here $\mathbf{V}^{(b)}$ is the velocity of baryons (the emitters and observers of radiation). Expression (1.13) is valid only in longitudinal gauge. The redshift perturbation is not gauge invariant. Only the total redshift, but not its background value is a measurable quantity. E.g. in the constant redshift time slicing, the redshift perturbation vanishes by definition.

To relate this to the CMB temperature fluctuation we have to take into account that the true, measured temperatures are the perturbed ones, $T_0 = \bar T_f + \delta T_f$ and $T_{\rm dec} = \bar T_i + \delta T_i$ so that

$$\frac{1}{1+\bar z} = \frac{a_i}{a_f} = \frac{\bar T_f}{\bar T_i} = \frac{T_0}{T_{\rm dec}}\left(1 - \frac{\delta T_f}{\bar T_f} + \frac{\delta T_i}{\bar T_i}\right) = \frac{T_0}{T_{\rm dec}}\left(1 - \frac{1}{4}\delta_\gamma\big|_i^f\right)\,, \tag{1.14}$$

where δ_r is the intrinsic density perturbation in the radiation and we have used $\rho_\gamma \propto T^4$ in the last equality. Inserting the above equation and Eq. (1.10) into Eq. (1.12), and using Eq. (5) for the definition of $h_{\mu\nu}$, one finds, after integration by parts, the following result for scalar perturbations:

$$\frac{E_f}{E_i} = \frac{T_0}{T_{\rm dec}}\left\{1 - \left[\frac{1}{4}D_g^{(r)} + V_j^{(b)}n^j + \Psi + \Phi\right]_i^f + \int_i^f (\dot\Psi + \dot\Phi)\, d\lambda\right\}\,. \tag{1.15}$$

Here $D_g^{(r)} = \delta_r - 4\Phi$ denotes the density perturbation in the radiation fluid in the constant curvature gauge, see [2] for more details.

Evaluating Eq. (1.15) at final time t_0 (today) and initial time $t_{\rm dec}$, we obtain the temperature difference of photons coming from different directions $\mathbf{n}_1$ and $\mathbf{n}_2$

$$\frac{\Delta T}{T} \equiv \frac{\Delta T(\mathbf{n}_1)}{T} - \frac{\Delta T(\mathbf{n}_2)}{T} \equiv \frac{E_f}{E_i}(\mathbf{n}_1) - \frac{E_f}{E_i}(\mathbf{n}_2)\,. \tag{1.16}$$

Direction-independent contributions to E_f/E_i do not enter in this difference.

The largest contribution to $\Delta T/T$ is the dipole term, $V_j^{(b)}(t_0)n^j$ which simply describes our motion with respect to the emission surface. Its amplitude is about 1.2×10^{-3} and it has been measured so accurately that even the yearly variation due to the motion of the Earth around the sun has been detected ($V_{\odot\oplus} \simeq 10^{-4}$).

For the higher multipoles (polynomials in n^j of degree 2 and higher) we can set

$$\frac{\Delta T(\mathbf{n})}{T} = \left[\frac{1}{4}D_g^{(r)} + V_j^{(b)}n^j + \Psi + \Phi\right](t_{\rm dec}, \mathbf{x}_{\rm dec}) + \int_{t_{\rm dec}}^{t_0} (\dot\Psi + \dot\Phi)(t, \mathbf{x}(t))\, dt\,, \tag{1.17}$$

where $\mathbf{x}(t) = \mathbf{x}_0 - \mathbf{n}(t_0 - t)$ is the unperturbed photon position at time t for an observer at $\mathbf{x}_0$, and $\mathbf{x}_{\rm dec} = \mathbf{x}(t_{\rm dec})$. The first term in Eq. (1.17) describes the intrinsic inhomogeneities of the radiation density on the surface of last scattering, due to acoustic oscillations prior to decoupling. Depending on the initial conditions, it can also contribute significantly on super-horizon scales. This is especially important in the case of adiabatic initial conditions. In a dust + radiation universe, adiabatic initial conditions imply $D_g^{(r)}(k,t) = -\frac{20}{3}\Psi(k,t)$ and $V^{(b)} = V^{(r)} \ll D_g^{(r)}$ when $kt \ll 1$. With $\Phi = \Psi$ the square bracket of Eq. (1.17) therefore gives for adiabatic perturbations

$$\left(\frac{\Delta T(\mathbf{n})}{T}\right)^{\rm (OSW)}_{\rm adiabatic} = \frac{1}{3}\Psi(t_{\rm dec}, \mathbf{x}_{\rm dec})\,, \tag{1.18}$$

on super-horizon scales. The contribution to $\Delta T/T$ from the last scattering surface on very large scales is called the 'ordinary Sachs–Wolfe effect' (OSW). It was derived for the first time by Sachs and Wolfe (1967) [3].

The second term in (1.17) describes the relative motion of emitter and observer. This is the Doppler contribution to the CMB anisotropies. It appears on the same angular scales as the acoustic term; we call the sum of the acoustic and Doppler contributions 'acoustic peaks'.

The integral in Eq. (1.17) accounts for the red- or blue shifts caused by the time dependence of the gravitational potential along the path of the photon, and represents the so-called integrated Sachs–Wolfe (ISW) effect. In a $\Omega = 1$, pure dust universe the Bardeen potentials are constant and there is no integrated Sachs–Wolfe effect; the blue shift which the photons acquire by falling into a gravitational potential is exactly cancelled by the redshift induced by climbing out of it. This is no longer true in a universe with substantial radiation contribution, curvature, or a cosmological constant. The sum of the ordinary Sachs–Wolfe term and the integral is the full Sachs–Wolfe contribution.

Similar results can be derived for vector and tensor perturbation, see [2].

1.3 CMB temperature anisotropy and polarisation power spectra

The CMB temperature anisotropy is a function on the sphere. It therefore makes sense to expand it in spherical harmonics,

$$\frac{\Delta T}{T}(\mathbf{x}_0, \mathbf{n}, t_0) = \sum_{\ell,m} a_{\ell m}(\mathbf{x}_0) Y_{\ell m}(\mathbf{n}) \,. \tag{1.19}$$

As a consequence of statistical isotropy off diagonal correlators of the $a_{\ell m}$'s vanish and we have

$$\langle a_{\ell m} \cdot a^*_{\ell' m'} \rangle = \delta_{\ell\ell'} \delta_{mm'} C_\ell \ . \tag{1.20}$$

The C_ℓs are the CMB power spectrum.

The 2-point correlation function, $\mathcal{C}(\mu)$, $\mu = \mathbf{n} \cdot \mathbf{n}'$, is related to the C_ℓs by

$$\begin{aligned}
\mathcal{C}(\mu) &\equiv \left\langle \frac{\Delta T}{T}(\mathbf{n}) \frac{\Delta T}{T}(\mathbf{n}') \right\rangle_{\mathbf{n}\cdot\mathbf{n}'=\mu} \\
&= \sum_{\ell,\ell',m,m'} \langle a_{\ell m} \cdot a^*_{\ell' m'} \rangle \, Y_{\ell m}(\mathbf{n}) Y^*_{\ell' m'}(\mathbf{n}') \\
&= \sum_\ell C_\ell \underbrace{\sum_{m=-\ell}^{\ell} Y_{\ell m}(\mathbf{n}) Y^*_{\ell m}(\mathbf{n}')}_{\frac{2\ell+1}{4\pi} L_\ell(\mathbf{n}\cdot\mathbf{n}')} \\
&= \frac{1}{4\pi} \sum_\ell (2\ell+1) C_\ell L_\ell(\mu) \ ,
\end{aligned} \tag{1.21}$$

where we have used the addition theorem of spherical harmonics for the last equality; the L_ℓs are the Legendre polynomials (see [4]).

Let us first discuss a simple but important case in somewhat more detail. We suppose the initial perturbations to be given by a spectrum of the form

$$\langle \Psi(\mathbf{k}, t) \Psi^*(\mathbf{k}', t') \rangle \, k^3 = (2\pi)^3 k^3 T_\Psi(k, t) T_\Psi(k, t') P_\Psi(k) \delta(\mathbf{k} - \mathbf{k}') \tag{1.22}$$

$$P_\Psi(k) = A_S (k t_0)^{n_s - 1} \ . \tag{1.23}$$

Here the transfer function at large scales is normalized to today $T_\Psi(0, t_0) \equiv 1$. We multiply by the constant $t_0^{n_s-1}$, the actual comoving size of the horizon, in order to keep A_S dimensionless for all values of n_s. The number n_s is called the spectral index. A_S then represents the amplitude of metric perturbations at horizon scale and larger today, $k < 1/t_0$.

Let us first only consider the ordinary Sachs Wolfe effect.

$$\frac{\Delta T}{T}(\mathbf{x}_0, \mathbf{n}, t_0) \simeq \frac{1}{3} \Psi(x_{\rm dec}, t_{\rm dec}) \ . \tag{1.24}$$

Since $\mathbf{x}_{\rm dec} = \mathbf{x}_0 + \mathbf{n}(t_0 - t_{\rm dec})$, the Fourier transform of (1.24) gives

$$\frac{\Delta T}{T}(\mathbf{k}, \mathbf{n}, t_0) = \frac{1}{3} \Psi(\mathbf{k}, t_{\rm dec}) \cdot e^{i\mathbf{k}\mathbf{n}(t_0 - t_{\rm dec})} \ . \tag{1.25}$$

Using the decomposition, see, e.g., [5],

$$e^{i\mathbf{k}\mathbf{n}(t_0 - t_{\rm dec})} = \sum_{\ell=0}^{\infty} (2\ell+1) i^\ell j_\ell(k(t_0 - t_{\rm dec})) L_\ell(\hat{\mathbf{k}} \cdot \mathbf{n}) \ , \tag{1.26}$$

where j_ℓ are the spherical Bessel functions [5] and $\hat{\mathbf{k}} = \mathbf{k}/k$, we obtain

$$\begin{aligned}
&\left\langle \frac{\Delta T}{T}(\mathbf{x}_0, \mathbf{n}, t_0) \frac{\Delta T}{T}(\mathbf{x}_0, \mathbf{n}', t_0) \right\rangle \qquad (1.27) \\
&= \frac{1}{(2\pi)^6} \int d^3k \, d^3k' \, e^{i\mathbf{x}_0 \cdot (\mathbf{k} - \mathbf{k}')} \left\langle \frac{\Delta T}{T}(\mathbf{k}, \mathbf{n}, t_0) \left(\frac{\Delta T}{T} \right)^* (\mathbf{k}', \mathbf{n}', t_0) \right\rangle \\
&\simeq \frac{1}{(2\pi)^6 9} \int d^3k d^3k' e^{i\mathbf{x}_0 \cdot (\mathbf{k} - \mathbf{k}')} \langle \Psi(\mathbf{k}, t_{\rm dec}) \Psi^*(\mathbf{k}', t_{\rm dec}) \rangle \sum_{\ell,\ell'=0}^{\infty} (2\ell+1)(2\ell'+1) i^{\ell - \ell'} \\
&\quad \cdot j_\ell(k(t_0 - t_{\rm dec})) j_{\ell'}(k'(t_0 - t_{\rm dec})) L_\ell(\hat{\mathbf{k}} \cdot \mathbf{n}) \cdot P_{\ell'}(\hat{\mathbf{k}}' \cdot \mathbf{n}') \\
&= \frac{1}{(2\pi)^3 9} \int d^3k P_\Psi(k, t_{\rm dec}) \sum_{\ell,\ell'=0}^{\infty} (2\ell+1)(2\ell'+1) i^{\ell - \ell'} \\
&\quad \cdot j_\ell(k(t_0 - t_{\rm dec})) j_{\ell'}(k(t_0 - t_{\rm dec})) L_\ell(\hat{\mathbf{k}} \cdot \mathbf{n}) \cdot P_{\ell'}(\hat{\mathbf{k}} \cdot \mathbf{n}') \ . \qquad (1.28)
\end{aligned}$$

In the first equals sign we have used the unitarity of the Fourier transformation. Inserting $L_\ell(\hat{\mathbf{k}}\mathbf{n}) = \frac{4\pi}{2\ell+1}\sum_m Y^*_{\ell m}(\hat{\mathbf{k}})Y_{\ell m}(\mathbf{n})$ and $P_{\ell'}(\hat{\mathbf{k}}\mathbf{n}') = \frac{4\pi}{2\ell'+1}\sum_{m'} Y^*_{\ell' m'}(\hat{\mathbf{k}})Y_{\ell' m'}(\mathbf{n}')$, integration over the directions $d\Omega_{\hat{k}}$ gives $\delta_{\ell\ell'}\delta_{mm'}\sum_m Y^*_{\ell m}(\mathbf{n})Y_{\ell m}(\mathbf{n}')$.

On large scales and in a matter dominated Universe on all scales Ψ is time independent so that we may neglect the transfer function, $T_\Psi(k,t) \simeq 1$ and $P_\Psi(k, t_{\rm dec}) \simeq P_\Psi(k)$.

Also using $\sum_m Y^*_{\ell m}(\mathbf{n})Y_{\ell m}(\mathbf{n}') = \frac{2\ell+1}{4\pi}L_\ell(\mu)$, where $\mu = \mathbf{n}\cdot\mathbf{n}'$, we find

$$\left\langle \frac{\Delta T}{T}(\mathbf{x}_0,\mathbf{n},t_0)\frac{\Delta T}{T}(\mathbf{x}_0,\mathbf{n}',t_0)\right\rangle_{\mathbf{n}\mathbf{n}'=\mu} \simeq \sum_\ell \frac{2\ell+1}{4\pi}L_\ell(\mu)\frac{2}{\pi}\int\frac{dk}{k}\frac{1}{9}P_\Psi(k)k^3 j^2_\ell(k(t_0-t_{\rm dec}))\ . \qquad (1.29)$$

Comparing this equation with Eq. (1.21) we obtain for *adiabatic perturbations* on scales $2 \le \ell \ll \chi(t_0 - t_{\rm dec})/t_{\rm dec} \sim 100$:

$$C_\ell^{(\rm SW)} \simeq C_\ell^{(\rm OSW)} \simeq \frac{2}{9\pi}\int_0^\infty \frac{dk}{k}P_\Psi(k)k^3 j^2_\ell\left(k\left(t_0-t_{\rm dec}\right)\right)\ . \qquad (1.30)$$

The function $j^2_\ell\left(k(t_0-t_{\rm dec})\right)$ peaks roughly at $k\left(t_0-t_{\rm dec}\right) \simeq kt_0 \simeq \ell$. If Ψ is a pure power law on large scales, $kt_{\rm dec} \lesssim 1$ as in Eq. (1.22) and we set $k(t_0 - t_{\rm dec}) \sim kt_0$, the integral (1.30) can be performed analytically. One finds

$$C_\ell^{(\rm SW)} = \frac{A_S}{9}\frac{\Gamma(3-n_s)\Gamma(\ell-\frac{1}{2}+\frac{n_s}{2})}{2^{3-n_s}\Gamma^2(2-\frac{n_s}{2})\Gamma(\ell+\frac{5}{2}-\frac{n_s}{2})} \quad \text{for } -3 < n_s < 3\ . \qquad (1.31)$$

Of special interest is the *scale-invariant* or Harrison–Zel'dovich (HZ) spectrum, $n_s = 1$. You have learned in Robert's course that inflationary initial conditions naturally generate a nearly scale invariant spectrum of scalar fluctuations. A HZ spectrum leads to

$$\ell(\ell+1)C_\ell^{(\rm SW)} = \frac{A_S}{9\pi} \simeq \left\langle\left(\frac{\Delta T}{T}(\vartheta_\ell)\right)^2\right\rangle\ , \quad \vartheta_\ell \equiv \pi/\ell\ . \qquad (1.32)$$

This is precisely (within the accuracy of the experiment) the behaviour observed by the DMR (differential microwave radiometer) experiment aboard

the satellite COBE [6]. The present much more precise estimation with the Planck satellite [1] shows statistically significant deviations from $n_s = 1$ to a slightly red spectrum as expected from standard inflationary models, $n_s = 0.965 \pm 0.004$.

Public codes like CAMB [7] and CLASS [8, 9] calculate the full CMB temperature anisotropy spectrum very efficiently with high accuracy (of about 0.1% for ΛCDM parameters not too far from the measured ones).

In Eq. (1.17) we have neglected the physics of last scattering which ir relevant on 'small' scales, $\ell > 200$ or so. We have assumed that last scattering is an infinitely thin instantaneous surface with $T \equiv T_{\rm dec}$. In reality, this surface has a certain thickness during which the scattering rate decreases from a very high value to below the Hubble rate. This leads to diffusion damping, called Silk damping in this context [10], on small scales. Furthermore, the finite thickness of the last scattering surface leads to projection effects which also damp fluctuations, see [2] for details. For these reasons, which are both important, the acoustic peaks of the fluctuation spectrum are damped on small scales, see Fig. 1.1.

Another important physical effect on the last scattering surface it the fact that polarisation is generated: The Thomson scattering cross section of a photon with polarisation in the scattering plane is suppressed by a factor $\cos^2\theta$, where θ denotes the scattering angle. Clearly, the transversality of photon polarisation requests that no photons with polarisation in the scattering plane can be scattered by 90^o. This would actually generate a longitudinal photon. Therefore, a quadrupole anisotropy of incoming photons on an electron leads to a net polarisation of the outgoing photons, see Fig. 1.2.

The generated polarisation pattern in the sky can be decomposed into so called E-polarisation which is parity even and B-polarisation which is parity odd and can only be generated by tensor modes. Since Thomson scattering does not generate circular polarisation, the polarisation tensor is a traceless symmetric spin-2 field in the sky which can be expanded in spin weighted spherical harmonics, see [2] for details,

$$P(\mathbf{n}) = \sum_{\ell m}\frac{1}{2}\left[(e_{\ell m}+b_{\ell m})\ {}_2Y_{\ell m}(\mathbf{n}) + (e_{\ell m}-b_{\ell m})\ {}_{-2}Y_{\ell m}(\mathbf{n})\right] \qquad (1.33)$$

Here the sum over ℓ starts at $\ell = 2$. Polarisation pattern for E and B-polarisation are shown in Fig. 1.3.

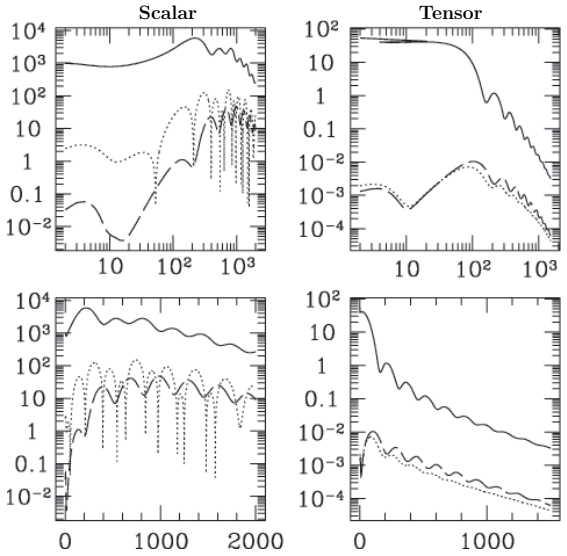

Figure 1.1: Scalar CMB anisotropy spectra are plotted for standard cosmological parameters. We show $\ell(\ell+1)C_\ell/(2\pi)$ in units of $(\mu K)^2$ as functions of ℓ in log-scale (top panels), where the Sachs–Wolfe plateau is clearly visible and in linear scale (bottom panels) which shows the equal spacing of the acoustic peaks. The solid line shows the temperature spectrum, the dashed line is the polarization and the dotted line shows the temperature–polarization cross correlation. The temperature–polarization cross correlation can become negative, the deep spikes in the dotted curves in the left-hand panels are actually sign changes (we show the absolute value in this log-plot). The left-hand side shows scalar fluctuation spectra, while the right-hand side shows tensor spectra. The observational data are well fitted by a purely scalar spectrum.

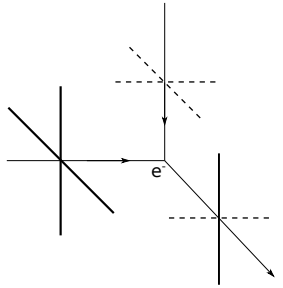

Figure 1.2: More incoming photons from the left than from the top (indicated in the figure with longer polarization directions), lead to a net polarization of the outgoing photon beam. In the situation shown above, where the scattering angle is $\pi/2$, the photons coming in from the left are scattered only if polarized vertically, while the photons coming in from the top are scattered only if polarized horizontally. In this way, an unpolarized photon distribution which exhibits a quadrupole anisotropy generates polarization on the surface of last scattering.

The E- and B-polariation spectra are given by

$$\langle e_{\ell m} e^*_{\ell' m'} \rangle = \delta_{\ell\ell'}\delta_{mm'} C^E_\ell \qquad \langle b_{\ell m} b^*_{\ell' m'} \rangle = \delta_{\ell\ell'}\delta_{mm'} C^B_\ell \tag{1.34}$$

The Kronecker deltas are again a consequence of statistical isotropy. Due to their different parity, E- and B-polarisation are uncorrelated, however temperature and E-polarisation are correlated, see Fig. 1.1.

Since scalar perturbations can only generate E-polarisation, the presence of B-polarisation is in principle a 'smoking gun' of tensor perturbations. However, this is not entirely true since we still have neglected one relevant physical mechanism which affects CMB temperature anisotropies and polarisation: lensing by foreground structures. This is actually a second order contribution but it has to be taken into account to achieve sufficiently accurate prediction for present day experiments. Lensing deflects photons so that a photon that comes in in a direction $\mathbf{n}$ has actually been emitted in a direction $\mathbf{n} - \boldsymbol{\alpha}$, where $\boldsymbol{\alpha}$ is called the deflection angle. A pure E-polarisation which is moved from its original position $\mathbf{n} - \boldsymbol{\alpha}$, to $\mathbf{n}$ actually acquires B polarisation. This B-polarisation has been measured in the CMB. Fortunately it dominates on small scales whereas B-polarisation from tensor modes is significant only on large scales (low ℓ). Therefore, it should be possible to subtract the B-polarisation signal from lensing with relatively good accuracy and measure tensor perturbations in future experiments if they are not too small (see next section).

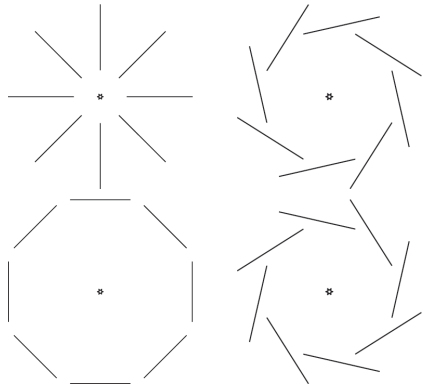

Figure 1.3: E-polarization (left) and B-polarization (right) patterns are shown around the photon direction indicated as the centre. E-polarization can be either radial or tangential, while B-polarization is of curl type.

1.4 Cosmological parameters from CMB observations

The scalar CMB spectra depend on the corresponding transfer functions,

$$C_\ell^X = \int T_X^2(\ell,k) k^3 P_\zeta(k) \frac{dk}{k} \tag{1.35}$$

Parametrizing the primordial power spectrum simply by an amplitude A_S and a spectral index n_s, the resulting spectra depend apart from these two parameters only on the cosmological parameters of the background model. Typically these are the baryon density, $\omega_b = \Omega_b h^2$, the cold dark matter (CDM) density $\omega_c = \Omega_c h^2$ and the cosmological constant, Ω_Λ. In a spatially flat Universe, the Hubble parameter, $H_0 = h100$km/sec/Mpc can then be inferred from the Friedmann constraint, $\Omega_b + \Omega_c + \Omega_\Lambda = 1$. An additional phenomenological parameter is the optical depth τ to the last scattering surface. Since the Universe is reionized at low redshift due to the UV radiation from the first stars, photons re-scatter somewhat. This slightly damps CMB anisotropies and re-generates some small amount of polarisation.

As an example of the physics of these parameters, let us consider the baryon density: Without baryons, the acoustic peaks in the CMB would be of equal height independent of the fact whether they are contraction peaks (maxima, the odd peaks) or expansion peaks (minima, the even peaks). Baryons, however are heavy and prefer clustering from expansion and therefore enhance the odd peaks and reduce the even peaks. This asymmetry is an excellent baryometer, see Fig. 1.4. The baryon density also has other effects: it determine the temperature of decoupling and Silk damping scale.

The position of the first acoustic peak is given by the ratio of the comoving distance to the last scattering surface and the comoving acoustic horizon at this surface,

$$\theta_{MC} \simeq \frac{r_s}{D_M} \tag{1.36}$$

$$r_s = \int_0^{t_{\rm dec}} c_s dt \tag{1.37}$$

$$D_M = \frac{1}{\sqrt{|\Omega_K|}H_0} \chi_K \left(\sqrt{|\Omega_K|} \int_0^{z_{\rm dec}} \frac{dz}{\Omega_m(1+z)^3 + \Omega_K(1+z)^2 + \Omega_\Lambda} \right) . \tag{1.38}$$

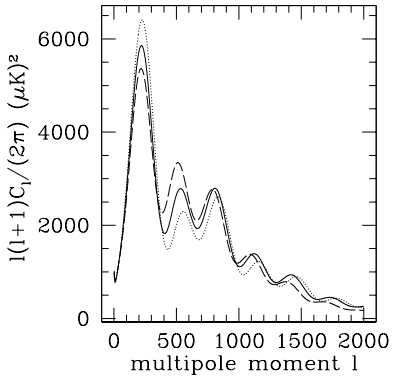

Figure 1.4: The CMB tempertura power spectrum for different values of $\Omega_b h^2$. At fixed $\Omega_{\rm cmd} h^2$ we show $\Omega_b h^2 = 0.02$ (solid), $\Omega_b h^2 = 0.03$ (dotted), $\Omega_b h^2 = 0.01$ (dashed).

Here we have included the curvature and introduced $\Omega_K = -K/(a_0 H_0)^2$. The function χ_K is the wellknown radial distance function given either by $\sinh\left(r/\sqrt{-K}\right)$, $\sin\left(r/\sqrt{K}\right)$ or r depending on the curvature. We have introduced this to stress that, without lensing, the CMB can measure very well the distance to the last scattering surface, but it cannot tell us whether this distance is generated by curvature, by a cosmological constant or by some other dark energy component. In principle the ISW effect is sensitive to this, but this term only contributes on large scale where the statistical error (cosmic variance) is significant and it can hardly be measured in the CMB. However, the lensing signal comes as we shall see in the next section, mainly from rather low redshifts, $z < 10$ and it breaks the degeneracy between Ω_K and Ω_Λ, see Fig. 1.5.

In order to find the best fit cosmological parameters one varies them (together with several unknown experimental nuisance parameters) minimizing a 'penalty function' or the log-likelihood. To search for the minimum and

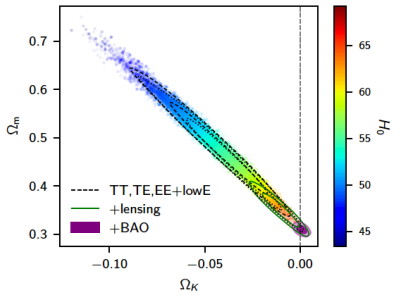

Figure 1.5: The Ω_m — Ω_K constraints from the Planck 2018 analysis. Figure from [1].

68% or 95% confidence contours one employs so called Markov-Chain Monte Carlo algorithms: One starts at some first guess value for the parameters, evaluates the penalty function, then makes a small step in parameter space and re-evaluates it. If the new penalty function is smaller, one keeps the new position, otherwise one drops it. And from there one starts over. There are many ways to improve this scheme and to avoid pitfalls. A very simple introduction and additional literature can be fund in [2]. To explore the likelihood surface, finding its maximum and 68% and 95% confidence contours, one needs typically of order 10^5 steps

In the simples case of fully diagonal Gaussian errors the $-\log$ of the likelihood is

$$\chi^2(\theta_1,\cdots,\theta_N) = \sum_\ell (C_\ell(\theta_1,\cdots,\theta_N) - C_\ell^{\rm obs})^2/\sigma_\ell^2\,. \tag{1.39}$$

Here the θ_i are the cosmological and the nuisance parameters and the σ_ℓ are the errors containing a statistical error $\sigma_\ell^{\rm stat}$ and an experimental error. The statistical error is given by

$$\sigma_\ell^{\rm stat} = \sqrt{\frac{2}{(2\ell+1)f_{\rm sky}}}C_\ell \qquad \text{(cosmic variance)}\,, \tag{1.40}$$

Parameter	Plik best fit	Plik [1]	CamSpec [2]	([2] − [1])/σ_1	Combined
$\Omega_b h^2$	0.022383	0.02237 ± 0.00015	0.02229 ± 0.00015	−0.5	0.02233 ± 0.00015
$\Omega_c h^2$	0.12011	0.1200 ± 0.0012	0.1197 ± 0.0012	−0.3	0.1198 ± 0.0012
$100\theta_{\rm MC}$	1.040909	1.04092 ± 0.00031	1.04087 ± 0.00031	−0.2	1.04089 ± 0.00031
τ	0.0543	0.0544 ± 0.0073	$0.0536^{+0.0069}_{-0.0077}$	−0.1	0.0540 ± 0.0074
$\ln(10^{10}A_s)$	3.0448	3.044 ± 0.014	3.041 ± 0.015	−0.3	3.043 ± 0.014
n_s	0.96605	0.9649 ± 0.0042	0.9656 ± 0.0042	+0.2	0.9652 ± 0.0042
$\Omega_m h^2$	0.14314	0.1430 ± 0.0011	0.1426 ± 0.0011	−0.3	0.1428 ± 0.0011
H_0 [km s^{-1}Mpc^{-1}]	67.32	67.36 ± 0.54	67.39 ± 0.54	+0.1	67.37 ± 0.54
Ω_m	0.3158	0.3153 ± 0.0073	0.3142 ± 0.0074	−0.2	0.3147 ± 0.0074
Age [Gyr]	13.7971	13.797 ± 0.023	13.805 ± 0.023	+0.4	13.801 ± 0.024
σ_8	0.8120	0.8111 ± 0.0060	0.8091 ± 0.0060	−0.3	0.8101 ± 0.0061
$S_8 \equiv \sigma_8(\Omega_m/0.3)^{0.5}$	0.8331	0.832 ± 0.013	0.828 ± 0.013	−0.3	0.830 ± 0.013
z_{re}	7.68	7.67 ± 0.73	7.61 ± 0.75	−0.1	7.64 ± 0.74
$100\theta_*$	1.041085	1.04110 ± 0.00031	1.04106 ± 0.00031	−0.1	1.04108 ± 0.00031
$r_{\rm drag}$ [Mpc]	147.049	147.09 ± 0.26	147.26 ± 0.28	+0.6	147.18 ± 0.29

Figure 1.6: The table of cosmological parameters estimated by the Planck experiment, from [1]. The upper part gives the directly estimated quantities, θ_{MC} is the angle subtended by the acoustic scale r_s

where $f_{\rm sky}$ denotes the sky fraction covered by the experment. Its maximal value is roughly 0.7 since data too close to the galactic plane cannot be used.

In Fig. 1.6 we show the cosmological parameters determined by the Planck experiment. These are the final values from 2018.

Before we move on, let me briefly also comment on a possible tensor (gravitational wave) contribution in the CMB spectra. This is usually cast in the so called 'tensor to scalar ratio which is defined as

$$r(k_*) = \frac{P_H(k_*)}{P_\zeta(k_*)}\,, \qquad k^3P_H(k) = A_T(k/k_*)^{n_t} \qquad k^3P_\zeta(k) = A_\zeta(k/k_*)^{n_s}\,, \tag{1.41}$$

where P_H denotes the gravitational wave power spectrum. Since both these spectra are (expected to be) close to scale invariant, the dependence on the 'pivot scale' k_* is mild. At present, the observed CMB polarisation B-modes are consistent with purely due to lensing, no tensor modes are detected in them. Since, however these data are still quite pure, the best upper limits on r come actually from a joint fit of the temperature anisotropies to a contribution from scalars + one from tensors. The present limit combining CMB and BAO data is [1]

$$r(0.002h/{\rm Mpc}) < 0.065\,. \tag{1.42}$$

Chapter 2

LSS

2.1 Introduction

At present, the best constraints for the model of our Universe still come from the CMB. Depending on experimental and modelling progress, this actually still may remain true for a couple years. But the CMB is essentially a two dimensional data set, while the galaxy distribution occupies our entire 3-dimensional past lightcone. If we can model and understand it sufficiently well, we can therefore learn much more not only about the parameters of the cosmological model, but also about gravity itself: is dark energy a manifestation of a break down of GR on very large scales (see Pedro's course)?

In this second chapter we therefore want to study observations of the galaxy distribution in detail. Thereby we shall always be very careful to distinguish between what is really observed and what we calculate. For example, how are galaxy counts in small angular and redshift bins related to density fluctuations?

However, before we come to this I want to give a brief introduction to weak lensing.

2.2 Weak lensing

In addition to shifting the energy of the photons, perturbations also deflect them. This phenomenon (as long as it is weak and does not lead to double images) is called weak lensing. We discuss it in this section at first order in perturbations.

2.2.1 The lens map

We consider a photon emitted in direction $\mathbf{n}$ from some source. Due to the metric perturbation the photon is deflected on its way to the observer and arrives in direction $n^i + \delta n^i$, where δn^i is given by Eq. (1.11). The first term, $-2n^j \Phi|_i^f$ is a contribution parallel to $\mathbf{n}$ and does not induce a deflection (it is necessary for the normalization of the perturbed geodesic). The second term contains a part normal to $\mathbf{n}$. Setting $\partial^i_\perp \equiv \partial^i - n^i n_j \partial^j$ the change of $\mathbf{n}$ normal to $\mathbf{n}$ is given by

$$\delta n^j_\perp|_i^f = -\int_i^f \partial^j_\perp(\Psi + \Phi)\, d\lambda\,. \tag{2.1}$$

Since the unperturbed affine parameter is $d\lambda = -dr$ we can convert this integral into an integral along the unperturbed (radial) line of sight (Born approximation). Using also that initially (at the source) $\delta \mathbf{n}_\perp = 0$ this yields

$$\delta n^j_\perp(r_s) = \int_0^{r_s} \partial^j_\perp(\Psi + \Phi)\, dr\,. \tag{2.2}$$

Here $r = 0$ is the final position (the one of the observer) and $r = r_s$ is the initial position, the one of the source. Let is first consider the special case where a deflection comes from only one point, say r along the line of sight. A deflection by an angle $\boldsymbol{\alpha}$ over a very short distance dr at r leads to a change at the observer by $d\alpha^j(r) = -d\delta n^j_\perp(r) = -\partial^j_\perp(\Psi + \Phi)dr$. (Note that we measure the deflection angle as seen from the observer while $\mathbf{n}$ is in the direction of propagation of the photon. This induces the minus sign.) The angular source position $\boldsymbol{\theta}$ in the sky is then deflected by an angle (exercise)

$$d\delta\theta^j(r) = \frac{r_s - r}{r_s} d\alpha^i = -\frac{(r_s - r)}{r_s}\partial^j_\perp(\Psi + \Phi)dr\,.$$

Integrating this deflection along the line of sight yields the (2-dimensional deflection angle

$$\delta\theta^j = -\int_0^{r_s} \frac{(r_s - r)dr}{r_s}\partial^j_\perp(\Psi + \Phi)\,. \tag{2.3}$$

Considering $\delta\theta$ as a function on the sphere and converting $\partial^j_\perp$ into angular derivatives, $\nabla_1 = \partial_\vartheta$ and $\nabla_2 = 1/(\sin\vartheta)^{-1}\partial_\varphi$ so that $\partial^a_\perp = r^{-1}\nabla^a$, we can rewrite this as

$$\delta\theta^a = -\nabla^a \int_0^{r_s} \frac{(r_s - r)dr}{r_s r}(\Psi + \Phi)\,. \tag{2.4}$$

The integral

$$\psi = -\int_0^{r_s} \frac{(r_s - r)dr}{r_s r}(\Psi + \Phi) = -2\int_0^{r_s} \frac{(r_s - r)dr}{r_s r}\Psi_W(t_0 - r, r, \vartheta, \varphi) \quad (2.5)$$

is called the lensing potential and we have introduced the Weyl potential,

$$\Psi_W = \frac{1}{2}(\Psi + \Phi) \simeq \Phi \simeq \Psi\,.$$

The near equal signs $\simeq$ are valid for perturbations with (nearly) vanishing anisotropic stress, like e.g. ΛCDM cosmology. The map

$$\theta \mapsto \theta + \delta\theta = \theta + \nabla\psi$$

is the lens map. For weak lensing, this map deviates only little from the identity. Its Jacobian is

$$\begin{aligned} A_{ab}(z, \vartheta, \varphi) &= \delta_{ab} + \nabla_a\nabla_b\psi(\vartheta, \varphi) = \delta_{ab} - 2\int_0^{r(z)} dr\, \frac{r(z) - r}{r(z)r}\nabla_a\nabla_b\Psi_W \\ &\equiv \begin{pmatrix} 1 - \kappa - \gamma_1 & -\gamma_2 \\ -\gamma_2 & 1 - \kappa + \gamma_1 \end{pmatrix}\,. \end{aligned} \quad (2.6)$$

The matrix A describes the deformation of a bundle of light rays from direction (ϑ, φ) and redshift z. Its trace, $\mathrm{tr}A = 2(1 - \kappa)$ is a measure for the amount of focusing while its traceless part is often represented as the complex number $\gamma = \gamma_1 + i\gamma_2$ represents the shear. As a double gradient of a scalar, A_{ab} is symmetric. To first order in perturbation theory, lensing from scalar perturbations does not induce rotation, which would be an anti-symmetric contribution to A.

After passing through the lensing potential, the intensity of a source $\iota(\mathbf{n}')$ becomes $\iota(\mathbf{n}) = \det(A^{-1})\iota(\mathbf{n}')$. With $\det(A^{-1}) = [(1 - \kappa)^2 - |\gamma|^2]^{-1} \simeq 1 + 2\kappa$, we obtain the magnification μ to first order in the gravitational potential,

$$\mu = 1 + 2\kappa\,. \quad (2.7)$$

Focusing not only increases the number of photons which reach us from a source (or a patch in the CMB sky), but it also enhances the solid angle under which we see this patch exactly by the factor $\det A$, so that the number of photons per unit solid angle is conserved. Lensing conserves surface

brightness. Photons are neither absorbed nor created by lensing, they are just deflected and redshifted.

The shear γ is very important for the weak lensing of galaxy surveys as it renders spherical sources elliptical. Correlating the ellipticity of galaxies which are close in angular position but not in radial, allows us the measure the foreground shear. The shear correlation function and power spectrum is one very important observable from galaxy surveys. At present, the best observations come from the DES [11] and Kids [12] surveys. These are very difficult observations which are still plagued by several problems, like, e.g. intrinsic alignment which are not yet fully under control. The convergence, κ, is very important for fluctuations of the luminosity distance and of number counts. For CMB lensing both, the focusing κ and the shear γ are relevant.

2.2.2 The lensing power spectrum

For scalar perturbations, the deflection angle is the gradient or the lensing or deflection potential. The deflection potential seems to be divergent at $r \to 0$. But this divergence affects only the constant monopole term which we may set to zero since it does not affect the lens map which is given by

$$A_{ab}(\vartheta, \varphi) = \delta_{ab} + \nabla_a\nabla_b\psi \qquad \text{with} \quad (2.8)$$

$$\kappa = -\frac{1}{2}\Delta_\Omega\psi \quad (2.9)$$

$$\gamma_1 = \frac{1}{2}(\nabla_1^2 - \nabla_2^2)\psi \quad (2.10)$$

$$\gamma_2 = -\nabla_1\nabla_2\psi\,. \quad (2.11)$$

Here Δ_Ω denotes the Laplacian on the sphere. Note that while κ is a scalar, $\gamma_\pm = \gamma_1 \pm i\gamma_2$ is a spin-2 tensor on the sphere with helicity $s = \pm 2$.

We consider a fixed radial position r_s or rather observed redshift z. We expand the lensing potential in spherical harmonics,

$$\psi(\mathbf{n}, z) = \sum_{\ell m} \psi_{\ell m}(z)Y_{\ell m}(\mathbf{n})\,. \quad (2.12)$$

We want to consider the correlation of the coefficients $\psi_{\ell m}(z)$ with other coefficients at a different redshift, $\psi_{\ell' m'}(z')$. As a consequence of statistical isotropy, coefficients with $\ell \neq \ell'$ or $m \neq m'$ are uncorrelated,

$$\langle\psi_{\ell m}(z)\bar{\psi}_{\ell' m'}(z')\rangle \equiv \delta_{\ell\ell'}\delta_{mm'}C_\ell^\psi(z, z')\,. \quad (2.13)$$

We use the addition theorem of spherical harmonics,

$$\sum_m Y_{\ell m}(\mathbf{n}) Y^*_{\ell m}(\mathbf{n}') = \frac{2\ell+1}{4\pi} L_\ell(\mathbf{n}\cdot\mathbf{n}')\,, \tag{2.14}$$

where L_ℓ denotes the Legendre polynomial or order ℓ. With this we obtain the lensing correlation function in terms of the power spectrum as

$$\langle \psi(\mathbf{n}, z)\psi(\mathbf{n}', z')\rangle = \frac{1}{4\pi}\sum_\ell (2\ell+1) C^\psi_\ell(z, z') L_\ell(\mathbf{n}\cdot\mathbf{n}')\ . \tag{2.15}$$

We now want to relate the lensing power spectrum to the primordial power spectrum of the Weyl potential. The power spectrum of the Weyl potential is given by the Fourier transform,

$$\Psi_W(t, \mathbf{x}) = \frac{1}{(2\pi)^3}\int d^3k\, \Psi_W(t, \mathbf{k})\, e^{-i\mathbf{k}\cdot\mathbf{x}}\ , \tag{2.16}$$

$$\langle \Psi_W(t, \mathbf{k})\Psi^*_W(t', \mathbf{k}')\rangle = (2\pi)^3 T(k, t)T^*(k, t')P_\Psi(k)\,\delta(\mathbf{k}-\mathbf{k}')\ . \tag{2.17}$$

Here we have introduced the primordial power spectrum P_Ψ and the linear transfer function $T(k, t)$. For a fixed wave number k the transfer function is the solution of the evolution equation for Ψ with initial condition $T(k, t) \to 1$ for $kt \to 0$. The linear transfer function for a ΛCDM universe, can be computed numerically with one of the standard codes CLASS or 'Camb' [8, 9, 7]. For simplicity, we neglect the difference between Ψ and Ψ_W which is given by the anisotropic stresses which are very small at late time in a ΛCDM universe. (This is not a vey good approximation for the CMB, but it is easily corrected for in a numerical treatment.)

Inserting Eqs. (2.17) and (2.5) in Eq. (2.15) and expanding

$$e^{i\mathbf{k}\cdot\mathbf{n}r} = 4\pi\sum_{\ell m} i^\ell j_\ell(kr) Y_{\ell m}(\mathbf{n}) Y^*_{\ell m}(\hat{\mathbf{k}}), \tag{2.18}$$

we obtain

$$C^\psi_\ell(z, z') = \frac{8}{\pi}\int_0^{r(z)} \frac{dr(r(z)-r)}{r(z)r}\int_0^{r(z')}\frac{dr'(r(z')-r')}{r(z')r'}\times \int_0^\infty dk k^2 T(k, t_0-r)T^*(k, t_0-r')j_\ell(kr)j_\ell(kr')P_\Psi(k)\,. \tag{2.19}$$

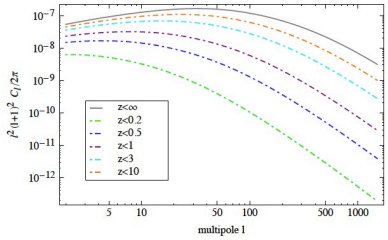

Figure 2.1: The linear lensing power spectrum for a ΛCDM concordance model out to different values of the redshift $z = z'$.

The relevant quantity for us is the spectrum of the deflection angle $\delta\theta(\mathbf{n}) = \nabla_\perp\psi(\mathbf{n})$. The correlation function of ψ only depends on the angle between $\mathbf{n}$ and $\mathbf{n}'$. It is invariant under simultaneous infinitesimal variations $\mathbf{n} \to \mathbf{n}+\boldsymbol{\epsilon}$ and $\mathbf{n}' \to \mathbf{n}'+\boldsymbol{\epsilon}$ so that $\langle\psi(\mathbf{n})\psi(\mathbf{n}'+\boldsymbol{\epsilon})\rangle = \langle\psi(\mathbf{n}-\boldsymbol{\epsilon})\psi(\mathbf{n}')\rangle$. Therefore $\langle\nabla_\perp\psi(\mathbf{n})\nabla_\perp\psi(\mathbf{n}')\rangle = -\langle\Delta\psi(\mathbf{n})\psi(\mathbf{n}')\rangle$. Since $\Delta Y_{\ell m} = -\ell(\ell+1)Y_{\ell m}$, the power spectrum of the deflection angle is simply given by $\ell(\ell+1)C^\psi_\ell$. This power spectrum, multiplied by the usual factor $\ell(\ell+1)/2\pi$, is shown in Fig. 2.1.

Another important quantity is the spectrum of κ wich is simply given by

$$C^\kappa_\ell(z, z') = [\ell(\ell+1)]^2 C^\psi_\ell(z, z')\,. \tag{2.20}$$

Expanding also the shear in spin-2 spherical harmonics one finds its power spectrum which perfectly agrees with the convergence one, see e.g. [13] for a derivation.

Limber approximation

Eq. (2.19) can be simplified by using the so called Limber approximation [14, 15],

$$\frac{2}{\pi}\int dk k^2 f(k) j_\ell(kr) j_\ell(kr') \simeq \frac{\delta(r-r')}{r^2} f\left(\frac{\ell+1/2}{r}\right)\,. \tag{2.21}$$

For a rather slowly varying function f with a converging k–integral this is a very good approximation for large enough values of ℓ. Here ℓ must be suffi-

ciently large so that $f(k)$ has no significant peak at $k > \ell/r$. For the Bardeen potential, $T^2(k,t)P_\Psi(k)$ this turns out to be a very good approximation for $\ell \gtrsim 20$.

Performing first the integral over k in (2.19) we obtain when using the Limber approximation

$$C_\ell^\psi(z,z') = 4\int_0^{r_*} dr \frac{(r(z)-r)(r(z')-r)}{r(z)r(z')r^4} T^2\left(\frac{\ell+1/2}{r}, t_0 - r\right) P_\Psi\left(\frac{\ell+1/2}{r}\right) , \tag{2.22}$$

where $r_* = \min\{r(z), r(z')\}$.

2.2.3 Exercises

Exercice 1
Consider an unperturbed spatially flat Friedmann universe, metric

$$ds^2 = a^2(-dt^2 + \delta_{ij}dx^i dx^j) .$$

Show that

$$(k^\mu) = \frac{\omega}{a^2}(1, \mathbf{n}) , \qquad \delta_{ij}n^i n^j \equiv \mathbf{n}^2 = 1 , \qquad \omega = \text{const.}$$

satisfies the photon geodesic equation, $(\omega/a^2)dk^\mu/d\lambda + \Gamma^\alpha_{\mu\nu}k_\mu k_\nu = 0$ and $g_{\mu\nu}k^\mu k^\nu = 0$ with affine parameter $\lambda = t$.
Hint: Compute the Christoffel's $\Gamma^\alpha_{\mu\nu}$ of the unperturbed metric.

Exercice 2
Show that up to a conformal factor, a perturbed Friedmann universe in longitudinal gauge has the metric

$$d\tilde{s}^2 = -(1+4\Psi_W)\, dt^2 + dr^2 + r^2(d\vartheta^2 + \sin^2\vartheta\, d\varphi^2) , \tag{2.23}$$

where

$$\Psi_W = \frac{1}{2}(\Psi + \Phi) . \tag{2.24}$$

Determine the conformal factor.
Compute the Christoffel symbols for (2.23) in the spherical coordinates $(t, r, \vartheta, \varphi)$.

Denoting the photon affine parameter by λ. Consider the perturbation of a geodesic which is radial in the background,

$$(\bar{t}, \bar{r}, \bar{\vartheta}, \bar{\varphi})) = (t_0 - \lambda_0 + \lambda, \lambda_0 - \lambda, \vartheta_0, \varphi_0) .$$

Show that to first order in the perturbations the angles ϑ and φ of the photon geodesic obey the equations

$$-\frac{d}{d\lambda}\left(r^2\frac{d}{d\lambda}\vartheta\right) = 2\partial_\vartheta\Psi_W , \tag{2.25}$$

$$-\frac{d}{d\lambda}\left(r^2\frac{d}{d\lambda}\varphi\right) = \frac{2}{\sin^2\vartheta}\partial_\varphi\Psi_W . \tag{2.26}$$

Using that $d\lambda = -dr$ to lowest order, show that to first order in Ψ_W these equations are solved by

$$\vartheta(r_*) = \vartheta_0 + 2\int_0^{r_*} dr\, \frac{(r_*-r)\partial_\vartheta\Psi_W(t_0 - r, r, \vartheta_0, \varphi_0)}{r_* r} , \tag{2.27}$$

$$\varphi(r_*) = \varphi_0 + \frac{2}{\sin^2\vartheta_0}\int_0^{r_*} dr\, \frac{(r_*-r)\partial_\varphi\Psi_W(t_0 - rt, r, \vartheta_0, \varphi_0)}{r_* r} . \tag{2.28}$$

Hint: The easiest way to see that these are the integrals of Eqs. (2.25) and (2.26) is to take the derivative of Eqs. (2.27) and (2.28) with respect to t_*

2.3 Perturbations of the luminosity distance

In this secton we derive the linear perturbation of the luminosity distance in a perturbed Friedmann Universe with vanishing curvature, $K = 0$. We follow the approach in [16] which considers perturbed photon geodesics and the Jacobi map, a simple consequence of the geodesic difference equation, see [17]. An alternative derivation using the optical scalars which we do not introduce here was developed by [18], where also the case $K \neq 0$ is discussed.

We start from the definition of the luminosity distance of a source at x_s^μ seen by an observer at x_o^μ,

$$d_L(o,s) = \left(\frac{L(x_s)}{4\pi F(x_o)}\right)^{1/2} . \tag{2.29}$$

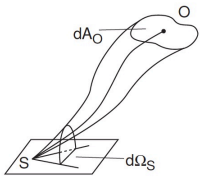

Figure 2.2: A light beam emitted at the source event S ending on the observer O. At the source position, the plane normal to the source four-velocity u_s is indicated.

This is a function of the direction $-\mathbf{n}$ of the source and of its redshift z which we now want to determine to first order in perturbation theory.

Be $d\Omega_s$ the infinitesimal solid angle around the source and $dA_o(x)$ the infinitesimal surface element on the surface normal to the photon beam at the position of the observer, x_o. The luminosity in direction $\mathbf{n}$ is then given by $4\pi dL(x_s)/d\Omega_s$ where the luminosity is $L = dE_s/d\tau_s$. The observed flux per unit area is $dF(x_o) = dE_o/d\tau_o/dA_o$. Introducing the redshift of the source, $1 + z = (k(\lambda_o) \cdot u_o)/(k(\lambda_s) \cdot u_s)$ we have $dE_s/dE_o = (1 + z)$ and $d\tau_o/d\tau_s = 1 + z$. We denote the photon 4-momentum by $k(\lambda)$ where λ denotes the affine parameter of the photon geodesic. Inserting these relations in (2.29) we find

$$d_L^2(o, s) = \frac{dA_o}{d\Omega_s}(1 + z)^2 = |\det J(o, s)|\,(1 + z)^2 \ . \tag{2.30}$$

Here J is the 2-dimensional Jacobi map. It is the projection of the 4 dimensional Jacobi map $\mathcal{J}$ into directions normal to the 4-velocity u and the photon direction n as defined below. The Jacobi map maps initial directions $\delta\theta_s^\alpha$ around the source into vectors δx_o^μ transversal to both the photon beam and the observer 4-velocity at the observer position as shown in Fig. 2.2, see [17] for more details,

$$\delta x_o^\mu = \mathcal{J}^\mu{}_\alpha(o, s)\delta\theta_s^\alpha \ . \tag{2.31}$$

To obtain the 2-dimensional Jacobi map we have to project $\mathcal{J}$ onto the

subspace normal to u and to the photon direction n given by

$$n_o = \frac{1}{\omega_o}\left(k(\lambda_o) + (k(\lambda_o) \cdot u_o)u_o\right) \quad \text{and} \tag{2.32}$$

$$n_s = \frac{1}{\omega_s}\left(k(\lambda_s) + (k(\lambda_s) \cdot u_s)u_s\right) \ . \tag{2.33}$$

The photon direction vectors n_s and n_o are normalized spacelike vectors pointing into the photon direction in the reference frame of the source at x_s and of the observer at x_o respectively. They should not be confused with the photon 4-velocity, which we also have denoted by n in the previous section and which is also divided by the frequency but which is in general not normal to u. The unperturbed spatial components, however agree.

To simplify the notation we also choose the photon momentum dimensionless by dividing by the unperturbed photon energy at emission such that $\bar{o}m_s \equiv \bar{o}m_o \equiv 1$. We then have $k^\mu = dx^\mu/d\lambda$.

Denoting the projectors onto the subspaces normal to u_s, n_s and u_o, n_o by P_s and P_o we have

$$(P_s)^\mu{}_\nu = \delta^\mu{}_\nu + u_s^\mu u_{s\nu} - n_s^\mu n_{s\nu} \quad \text{and} \tag{2.34}$$

$$(P_o)^\mu{}_\nu = \delta^\mu{}_\nu + u_o^\mu u_{o\nu} - n_o^\mu n_{o\nu} \ . \tag{2.35}$$

The Jacobi map is $J(o, s) = P_o\mathcal{J}(o, s)P_s$, understood as a two dimensional linear map. For convenience we shall write it as four-dimensional map and determine its determinant as the product of the two non-vanishing eigenvalues.

To find the Jacobi map we have to derive a differential equation which relates $\delta\theta^\alpha$ to δx^β. A short calculation using the geodesic difference equation for photon propagation yields (see [17] and [16])

$$\nabla_k(\omega_s\delta\theta^\alpha) = R^\alpha_{\beta\mu\nu}k^\beta k^\mu\delta x^\nu \tag{2.36}$$

$$\nabla_k(\delta x^\alpha) = \omega_s\delta\theta^\alpha \ . \tag{2.37}$$

Using the definition of the covariant derivative this gives

$$\omega_s\frac{d(\delta x^\alpha)}{d\lambda} = -\Gamma^\alpha_{\mu\nu}k^\mu\delta x^\nu + \omega_s\delta\theta^\alpha \equiv C^\alpha_\nu(\lambda)\delta x^\nu + \omega_s\delta\theta^\alpha \tag{2.38}$$

$$\frac{d(\omega_s\delta\theta^\alpha)}{d\lambda} = R^\alpha_{\beta\mu\nu}k^\beta k^\mu\delta x^\nu - \Gamma^\alpha_{\mu\nu}k^\mu\omega_s\delta\theta^\nu \equiv A^\alpha_\nu(\lambda)\delta x^\nu + C^\alpha_\nu(\lambda)\omega_s\delta\theta^\nu \tag{2.39}$$

where we have set

$$\omega_s C^\alpha_\beta(\lambda) = -\Gamma^\alpha_{\mu\beta}k^\mu \quad \text{and} \quad \omega_s^2 A^\alpha_\beta(\lambda) = R^\alpha_{\rho\mu\beta}k^\rho k^\mu \,. \tag{2.40}$$

We have also used that the background wave vector is simply $(\bar{k}^\mu) = \omega_s(1, \mathbf{n})$ and we have introduced for a first order perturbation f $\quad (\dot{f} \equiv \partial_t f)$

$$\frac{df}{d\lambda} = \dot{f} + n^i \partial_i f \,. \tag{2.41}$$

The initial conditions are $\delta x^\alpha(\lambda_s) = 0$ since all photons start from the same source event and $(k^\alpha \cdot \delta\theta_\alpha)(\lambda_s) = (u_s^\alpha \cdot \delta\theta_\alpha(\lambda_s)) = 0$ since the transverse directions at the source are normal to u_s and k_s. The solution of Eqs. (2.38) and (2.39) therefore provides a linear relation between the initial condition $\delta\theta^\alpha(\lambda_s)$ and $\delta x^\alpha(\lambda)$,

$$\delta x^\alpha(\lambda) = \mathcal{J}^\alpha_\beta(\lambda)\delta\theta^\beta(\lambda_s) \,. \tag{2.42}$$

With $\mathcal{J}(\lambda_o)$ we can then determine the true Jacobi map $J(o,s) = P_o\mathcal{J}(\lambda_o)P_s$.

We now use the fact that the perturbed Friedmann metric (denoted by a tilde like in the previous section) is conformally related to perturbed Minkowski spacetime. Therefore, the two have the same lightlike geodesics, only the affine parameters are different. They are related by (see Section 1.2)

$$\frac{d\tilde{\lambda}}{d\lambda} = a^2 \,,$$

while the velocities are related by $u = a\tilde{u}$ so that the redshifts are related by

$$1 + \tilde{z} = \frac{a_o}{a_s}(1+z) \,. \tag{2.43}$$

Keeping these relations in mind, we can perform the calculation in perturbed Minkowski space. Our result (1.13) for the redshift perturbation still holds. For the Christoffel symbols and the Riemann tensor to first order we can use the results of Appendix 3 of Ref. [2] by simply setting $\mathcal{H} = K = 0$ or by

solving Exercise 1 of this section. This yields

$$\begin{aligned}
C^0_0 &= -\frac{d\Psi}{d\lambda} \\
C^0_i &= -\partial_i\Psi + \dot{\Phi}n^i = C^i_0 \\
C^i_j &= \frac{d\Psi}{d\lambda}\delta^i_j + n^i\partial_j\Phi - n^j\partial_i\Phi \qquad (2.44) \\
A^0_0 &= \ddot{\Phi} + n^i n^j \partial_i\partial_j\Psi \\
A^0_i &= -\frac{d}{d\lambda}(n^i\dot{\Phi} - \partial_i\Psi) + \partial_i(\dot{\Phi} + \dot{\Psi}) = -A^i_0 \\
A^i_j &= -\frac{d^2\Phi}{d\lambda^2}\delta^i_j - \partial_j\partial_i(\Phi + \Psi) + \frac{d\partial_j\Phi}{d\lambda}n^i + \frac{d\partial_i\Phi}{d\lambda}n^j \,. \qquad (2.45)
\end{aligned}$$

Spatial indices i or j are raised and lowered with the flat metric δ_{ij}. Therefore, no special attention is paid to their position.

To zeroth order, the photons move along straight lines and the energy is not redshifted so that we simply obtain $\delta\bar{\theta}^\alpha(\lambda) = \delta\theta^\alpha_s$, $\bar{\omega}(\lambda) = \omega_s$ and $\delta\bar{x}^\alpha(\lambda) = (\lambda - \lambda_s)\delta\bar{\theta}^\alpha_s$. For the Jacobi map this implies $\bar{\mathcal{J}}^\alpha_\beta = (\lambda_o - \lambda_s)\delta^\alpha_\beta$. The projector onto the tangent space normal to the observer velocity and the photon direction is simply $\bar{P}_s = \bar{P}_o = \bar{P}$, where

$$\begin{aligned}
\bar{P}^0_0 &= \bar{P}^0_i = \bar{P}^i_0 = 0 \\
\bar{P}^i_j &= \delta^i_j - n^i n_j \,. \qquad (2.46)
\end{aligned}$$

The zeroth order 2-dimensional Jacobi map is therefore given by $\bar{J}^\alpha_\beta = (\bar{P}\bar{\mathcal{J}}\bar{P})^\alpha_\beta$

$$\begin{aligned}
\bar{J}^0_0 &= \bar{J}^0_i = \bar{J}^i_0 = 0 \\
\bar{J}^i_j &= (\lambda_s - \lambda_s)\left(\delta^i_j - n^i n_j\right) \,. \qquad (2.47)
\end{aligned}$$

The 2-dimensional determinant of the Jacobi map is therefore $\det\bar{J} = (\lambda_o - \lambda_s)^2$, leading to the flat space luminosity distance $d_L = \lambda_o - \lambda_s = t_o - t_s$.

Since C and A are already first order, the first order differential equation becomes

$$\begin{aligned}
\frac{d}{d\lambda}\delta x^{\alpha\,(1)}(\lambda) &= C^{\alpha\,(1)}_\beta(\lambda)\delta\bar{x}^\beta(\lambda) + (\delta\theta^\alpha)^{(1)}(\lambda) \\
\frac{d}{d\lambda}(\delta\theta^\alpha)^{(1)}(\lambda) &= A^{\alpha\,(1)}_\beta(\lambda)\delta\bar{x}^\beta(\lambda) + C^{\alpha\,(1)}_\beta(\lambda)\delta\bar{\theta}^\beta(\lambda) \,.
\end{aligned} \tag{2.48}$$

Making use of the background solution we obtain

$$
\begin{aligned}
(\delta\theta^\alpha)^{(1)}(\lambda) &= \int_{\lambda_s}^{\lambda} d\lambda' \left(A^\alpha_\beta(\lambda')(\lambda'-\lambda_s) + C^\alpha_\beta(\lambda')\right)(\delta\bar\theta^\beta_s) + (\delta\theta^\alpha_s)^{(1)} \qquad (2.49)\\
\delta x^{\alpha\,(1)}(\lambda) &= \left[\int_{\lambda_s}^{\lambda} d\lambda' C^\alpha_\beta(\lambda')(\lambda'-\lambda_s) + \right.\\
&\quad \left.\int_{\lambda_s}^{\lambda} d\lambda' \int_{\lambda_s}^{\lambda'} d\lambda'' \left(A^\alpha_\beta(\lambda'')(\lambda''-\lambda_s) + C^\alpha_\beta(\lambda'')\right)\right]\bar\omega_s\delta\bar\theta^\beta_s\\
&\quad +(\lambda-\lambda_s)(\omega_s\delta\theta^\alpha_s)^{(1)}\ . \qquad (2.50)
\end{aligned}
$$

We can define the initial conditions such that $(\delta\theta^\alpha_s)^{(1)} = 0$. The first order contribution to the unprojected Jacobi map then becomes

$$
\begin{aligned}
\mathcal{J}^{\alpha\,(1)}_\beta(\lambda_o) &= \int_{\lambda_s}^{\lambda_o} d\lambda C^\alpha_\beta(\lambda)(\lambda-\lambda_s) + \\
&\quad \int_{\lambda_s}^{\lambda_o} d\lambda \int_{\lambda_s}^{\lambda} d\lambda' \left(A^\alpha_\beta(\lambda')(\lambda'-\lambda_s) + C^\alpha_\beta(\lambda')\right)\ . \qquad (2.51)
\end{aligned}
$$

We want to compute $J^{(1)}$

$$
J^{(1)\,\alpha}{}_\beta = (P_o\mathcal{J}P_s)^{(1)\,\alpha}{}_\beta = \bar P^\alpha_\mu \mathcal{J}^{(1)\,\mu}{}_\nu \bar P^\nu_\beta + P^{(1)}_{o\,\mu}{}^\alpha \bar{\mathcal{J}}^\mu_\nu \bar P^\nu_\beta + \bar P^\alpha_\mu \bar{\mathcal{J}}^\mu_\nu P^{(1)\,\nu}_{s\,\beta}\ . \quad (2.52)
$$

A short calculation, inserting our results for C and A gives

$$
(\bar P\mathcal{J}\bar P J)^i{}_j = U\left(\delta^i_j - n^i n_j\right) + W^i_j - n^i n^k W_{kj} - n_j n^k W^i_k + n^i n_j n^k n^l W_{kl}
$$

with

$$
\begin{aligned}
U &= -2\Psi_s(\lambda_o-\lambda_s) + 2\int_{\lambda_s}^{\lambda_o} d\lambda\Phi(\lambda) \quad \text{and}\\
W_{ij} &= -\int_{\lambda_s}^{\lambda_o} d\lambda \int_{\lambda_s}^{\lambda} d\lambda' \partial_i\partial_j[\Psi(\lambda')+\Phi(\lambda')](\lambda'-\lambda_s)\ . \qquad (2.53)
\end{aligned}
$$

Implicit summation over repeated (spatial) indices is assumed and $n^i = n_i$, $W^i_j = W_{ij} = W^{ij}$.

Calculating also the first order contributions to the projections, inserting (1.10) and (1.11) for the perturbed photon momentum, we obtain

$$
\begin{aligned}
J^0_0 &= 0\\
J^0_i &= \omega_s(\lambda_o-\lambda_s)\left(v^i_o - n^i n_k v^k_o\right)\\
J^i_0 &= \omega_s(\lambda_o-\lambda_s)\left(-v^i_s + n^i n^k v^k_s\right)\\
J^i_j &= \omega_s(\lambda_o-\lambda_s)\Bigg\{\left(1-2\Psi_s + \frac{1}{\lambda_o-\lambda_s}\int_{\lambda_s}^{\lambda_o} d\lambda[\Psi+\Phi]\right)\delta^i_j\\
&\quad +n^i n_j\Bigg(-1+2\Psi_s - \frac{1}{\lambda_o-\lambda_s}\int_{\lambda_s}^{\lambda_0} d\lambda[\Psi+\Phi]\\
&\quad -\mathbf{n}(\mathbf{v}_o+\mathbf{v}_s) - \int_{\lambda_s}^{\lambda_0} d\lambda\nabla[\Psi+\Phi]\mathbf{n}\Bigg) + n^i v_{o\ j} + n_j v^i_s\\
&\quad +\int_{\lambda_s}^{\lambda_0} d\lambda\partial_j[\Psi+\Phi]n^i - \frac{1}{\lambda_0-\lambda_s}\int_{\lambda_s}^{\lambda_0} d\lambda\int_{\lambda_s}^{\lambda} d\lambda'(\lambda'-\lambda_s)\Bigg(\partial_i\partial_j\\
&\quad -n^i n^k\partial_j\partial_k - n^j n^k\partial_i\partial_k + n^i n^j n^k n^l\partial_k\partial_l\Bigg)[\Psi+\Phi]\Bigg\}\ . \qquad (2.54)
\end{aligned}
$$

Like in the unperturbed case, the two eigenvalues of the Jacobi map are equal. This is due to the fact that the shear contribution to the Jacobi map still vanishes at first order. A short computation gives the eigenvalues α,

$$
\begin{aligned}
\alpha = \omega_s(\lambda_o-\lambda_s)\Bigg\{&1-2\Psi_s + \frac{1}{\lambda_o-\lambda_s}\int_{\lambda_s}^{\lambda_o} d\lambda(\Phi+\Psi) -\\
&\frac{1}{2(\lambda_o-\lambda_s)}\int_{\lambda_s}^{\lambda_o} d\lambda\int_{\lambda_s}^{\lambda} d\lambda'(\lambda'-\lambda_s)\Big(\nabla^2 - n^i n^j\partial_i\partial_j\Big)[\Psi+\Phi]\Bigg\}\ . \qquad (2.55)
\end{aligned}
$$

The luminosity distance of the perturbed Minkowski spacetime is given by $d_L = (\omega_s/\omega_o)\alpha$. Inserting the above expressions and taking into account the perturbation of the redshift, $\omega_s/\omega_o = 1+\delta z$, and $\omega_s = -(g_{\mu\nu}k^\mu u^\nu)_s = 1-\Psi_s - \mathbf{n}\cdot\mathbf{v}_s$, we obtain

$$d_L = (t_o - t_s)\Bigg\{1 - (3\Psi_o - \Phi_o) + 2\Psi_s - \Phi_s + \mathbf{n}\cdot(\mathbf{v}_o - 2\mathbf{v}_s) + \frac{1}{t_o - t_s}\int_{t_s}^{t_o} dt(\Psi + \Phi) + \int_{t_s}^{t_o} dt\mathbf{n}\cdot\nabla(\Psi + \Phi) + \frac{1}{t_o - t_s}\int_{t_s}^{t_o} dt\int_{t_s}^{t} dt'\mathbf{n}\cdot\nabla(\Psi + \Phi) \frac{-1}{2(t_o - t_s)}\int_{t_s}^{t_o} dt\int_{t_s}^{t} dt'(t' - t_s)\Big(\nabla^2(\Psi + \Phi) - \partial_i\partial_j(\Psi + \Phi)n^i n^j\Big)\Bigg\}. \tag{2.56}$$

Here we have also transformed the parameter λ into the conformal time t via the relation

$$\frac{dt}{d\lambda} = n^0(\lambda) = 1 + (\Phi - \Psi)|_s^o - \int_{\lambda_s}^{\lambda_o} d\lambda\mathbf{n}\cdot\nabla(\Psi + \Phi)\,.$$

Note that d_L is not just a function of $v_s - v_o$. This comes from the fact that the Jacobi map itself depends on $\mathbf{v}_s$ but not on $\mathbf{v}_o$, see [17].

To simplify this expression we note that the transverse (angular) Laplacian is given by

$$\nabla_\perp^2 = \big(\partial_i - n_i(n^j\partial_j)\big)^2 = \partial_i\partial^i - n^i n^j\partial_i\partial_j - \frac{2}{r}n^i\partial_i = r^{-2}\Delta_\Omega\,, \tag{2.57}$$

where Δ_Ω denotes the Laplacian on the 2-sphere and $r = t' - t_s$ is the distance from the source. With this the doubly integrated terms become $(t' - t_s)\Delta_\Omega(\Phi + \Psi)$. We also perform the integration by parts,

$$\int_{t_s}^{t_o} dt\int_{t_s}^{t} dt'(t' - t_s)f(t') = \int_{t_s}^{t_o} dt(t - t_s)(t_o - t)f(t)\,.$$

With this we find

$$d_L(t_s) = (t_o - t_s)\Bigg\{1 - (3\Psi_o - \Phi_o) + 2\Psi_s - \Phi_s + \mathbf{n}\cdot(\mathbf{v}_o - 2\mathbf{v}_s)\Bigg\} + \int_{t_s}^{t_o} dt(\Psi + \Phi) + \frac{1}{2}\int_{t_s}^{t_o} dt\frac{(t - t_s)}{t_o - t}\Delta_\Omega(\Psi + \Phi)\,. \tag{2.58}$$

We now take into account expansion, which gives $\tilde{d}_L = \frac{a_o^2}{a_s}d_L = a_s^{-1}d_L$, we normalize $a_o = 1$. Furthermore, we neglect the gauge dependent monopole

and dipole terms, Ψ_o and $\mathbf{n}\cdot\mathbf{v}_o$. Transforming the time integral into a radial intgral with $r = t_0 - t$ and $dr = -dt$ we then find the following result for the luminosity distance in an perturbed Friedmann universe

$$\tilde{d}_L(t_s, \mathbf{n}) = \frac{r_s}{a_s}\Bigg\{1 + 2\Psi_s - \Phi_s - 2\mathbf{n}\cdot\mathbf{v}_s + \frac{1}{r_s}\int_0^{r_s} dr(\Psi + \Phi) + \frac{1}{2}\int_0^{r_s} dr\frac{(r_s - r)}{r_s r}\Delta_\Omega(\Psi + \Phi)\Bigg\}. \tag{2.59}$$

Eq. (2.59) is the luminosity distance of a source in direction $-\mathbf{n}$ emitted at conformal distance r_s at time $t_s = t_0 - r_s$. However, this quantity is not directly measurable. What we do measure instead is the redshift of the source, $z_s = \bar{z}_s + \delta z_s$, where $\bar{z}_s + 1 = 1/a(t_s)$. Now

$$\tilde{d}_L(t_s, \mathbf{n}) = \tilde{d}_L(t(\bar{z}_s), \mathbf{n}) \equiv \tilde{d}_L(\bar{z}_s, \mathbf{n}) = \tilde{d}_L(z_s, \mathbf{n}) - \frac{d}{d\bar{z}_s}\tilde{d}_L(z_s, \mathbf{n})\delta z_s\,. \tag{2.60}$$

Furthermore, from the background expression for the luminosity distance we infer

$$\frac{d}{d\bar{z}_s}\tilde{d}_L(z_s, \mathbf{n}) = (1 + z_s)^{-1}\tilde{d}_L + \mathcal{H}_s^{-1} + \text{ first order.} \tag{2.61}$$

Inserting this in Eq. (2.59), using expression (1.13) for δz, yields

$$\frac{\delta d_L(z_s, \mathbf{n})}{\bar{d}_L(z_s)} = -\Phi_s - \left(1 - \frac{1}{\mathcal{H}_s r_s}\right)\left[\Psi_s + \mathbf{n}\mathbf{v}_s + \int_0^{r_s} dr(\dot{\Psi} + \dot{\Phi})\right] + \int_0^{r_s}\frac{dr}{r_s}\left[1 - \frac{(r - r_s)}{2r}\Delta_\Omega\right](\Psi + \Phi)\,. \tag{2.62}$$

The second integrated term is the Shapiro time delay minus the convergence κ. The first integrated term is the integrated Sachs Wolfe term which appears also in CMB anisotropies. The non-integrated terms are contributions from the gravitational potential at the source and the Doppler term. Corresponding terms at the observer have been neglected as they contribute just gauge dependent monopole and dipole terms.

This result will be important for the number count perturbations discussed in the next section.

In [16] and [18] it is also shown that the expression (2.62) is gauge invariant, as we expect if for a measurable quantity. Only the monopole, which has a non-vanishing background contribution is not gauge invariant.

2.3.1 Exercice

Compute the Christoffel symbols and the Riemann tensor in a perturbed Minkowski space with metric

$$ds^2 = -(1+2\Psi)dt^2 + (1-2\Phi)\delta_{ij}dx^i dx^j$$

to first order in Φ and Ψ.

2.4 Galaxy number counts

2.4.1 Introduction

The large scale matter distribution (large scale structure or LSS) of the Universe is an interesting observable which is widely used to determine not only the properties of our Universe but also to test the theory of gravitation, General Relativity itself. In this section we discuss observations of LSS from a fully relativistic point of view. We first make contact with the standard non-relativistic treatment and briefly discuss its merits and its shortcomings. Then we develop a relativistic analysis which has much in common with the study of the CMB, see [2]. In the last sub-section, we briefly also discuss intensity mapping, a new, promising technique to observe LSS or, more generally, the distribution of neutral hydrogen.

LSS is more complicated than the CMB since we usually observe the distribution of galaxies, discrete, nonlinear over-dense spots in the sky which we approximate as points in this context. On the other hand, we calculate the matter over density and the relation between these two quantities is what we call 'bias'. Galaxies are a discrete biased tracer of the density field. We have good reasons to believe that on large scales bias is linear and scale independent, but we expect it to depend on redshift. Here we concentrate on these large scales, since we treat the problem within linear perturbation theory which is valid only on sufficiently large scales and at sufficiently high redshift. Furthermore, the relativistic treatment which is the novelty of the present treatment is relevant mainly on large scales.

In the past, observers usually surveyed a rather small region in the sky and considered the observed galaxy number density in some volume element $r^2 dr d\Omega$ as proportional to the matter density $\rho(t)(1+\delta(\mathbf{x},t))$. They then performed a discrete Fourier transform on this dataset to infer the power spectrum. The details of this procedure can be found e.g. in [19]. For small regions this is actually sufficient (apart from redshift space distortions which we discuss below and which are nowadays also included in the analysis). However, when we go out to large redshifts and/or observe large patches in the sky, we have to take into account that observations are made on the background lightcone and not in a spatial volume. We also have to take into account that with the perturbed metric, this background lightcone is also perturbed.

What we truly observe of a galaxy is its direction in the sky, $-\mathbf{n}$ (like in Section 1.2, $\mathbf{n}$ is the propagation direction of the incoming photon), and its redshift, z. The measured over-density is therefore a quantity of the form $\Delta(\mathbf{n}, z)$ and in this section we want to compute it and to relate it to $\delta(\mathbf{x}, t)$ and other perturbation variables.

Be $N(\mathbf{n}, z)$ the number of galaxies in an small solid angle $d\Omega$ around $\mathbf{n}$ and in a redshift bin $[z, z+dz]$. We define the number count fluctuation as

$$\Delta(\mathbf{n}, z) = \frac{N(\mathbf{n}, z) - \bar{N}(z)}{\bar{N}(z)}\,. \tag{2.63}$$

Here $4\pi f_{\rm sky}\bar{N}(z)$ is the total number of galaxies observed in the redshift bin $[z, z+dz]$ and $f_{\rm sky}$ denotes the observed sky fraction. $\Delta(\mathbf{n}, z)$ is a truly observable quantity and therefore its expression within linear perturbation theory is gauge invariant.

We expand the angular dependence of Δ in terms of spherical harmonics,

$$\Delta(\mathbf{n}, z) = \sum_{\ell,m} a_{\ell m}(z) Y_{\ell m}(\mathbf{n})\,. \tag{2.64}$$

The corresponding power spectra are

$$\langle a_{\ell m}(z) a^*_{\ell' m'}(z')\rangle = C_\ell(z, z')\delta_{\ell\ell'}\delta_{mm'}\,. \tag{2.65}$$

Like in Section 2.2.2, the Kronecker-deltas are a consequence of statistical isotropy and we have a density field at arbitrary redshift and different redshifts are not uncorrelated. As we shall see below, the correlation of different redshifts is an excellent mean to determine the lensing convergence κ introduced in Eq. (2.6).

2.4.2 Redshift space distortion and lensing

Before we derive the full relativistic expression for the number count fluctuations, we consider the quasi-Newtonian situation. We also do not pay attention to gauge issues and the result we derive here is actually not gauge invariant. However, on scales mucvh smaller than the Hubble scales, gauge transformations have no significant effect, see e.g. [2]. The only relativistic term we take into account in a second step is the deflection of the light coming from our galaxies, i.e. lensing. We consider objects (e.g. galaxies or a certain class of galaxies) with a density which is proportional to the matter density. Neglecting first this proportionality factor (the bias), its fluctuation is given by

$$N(\mathbf{n},z) = \rho(\mathbf{n},z)V(\mathbf{n},z) = \bar{\rho}\bar{V}\left(1+\delta_z+\frac{\delta V}{V}\right)\,, \tag{2.66}$$

where δ_z denotes the density fluctation at fixed redshift. In addition to the naively expected fluctuation of the observed number in a small volume V, we also have to take into account the fluctuation of the volume element itself. For a given direction at the observer, $\mathbf{n}$, and observed redshift z, the volume element is

$$V = r^2(z)d\Omega_{\mathbf{n}}dr = r^2(z)\frac{dr}{dz}d\Omega_{\mathbf{n}}dz\,. \tag{2.67}$$

Redshift space distortion

In an unperturbed Friedmann universe, r is simply the comoving distance of the emitter at redshift z, $r(z)=\int_0^z H^{-1}(z')dz'$ and $dr/dz = H^{-1}(z) = a/\mathcal{H}$. In a perturbed Universe, both r and z acquire perturbations. In a Newtonian setting only z is perturbed by the Doppler effect and we have $z=\bar{z}+\delta z$ with

$$\frac{\delta z}{1+\bar{z}} \;=\; -\mathbf{V}(z)\cdot\mathbf{n} = V_r\,. \tag{2.68}$$

In this Newtonian treatment we neglect Sachs Wolfe and integrated Sachs Wolfe effects which are taken into account in Eq. (1.13) and which we shall also consider in the next section.

In our derivative above we have to insert $dz = d\bar{z}(1+d\delta z/d\bar{z})$ or

$$\frac{dr}{dz} = \left(1-\frac{d\delta z}{d\bar{z}}\right)\frac{dr}{d\bar{z}} = \frac{1}{(1+z)\mathcal{H}}\left(1+\mathbf{V}\cdot\mathbf{n}+\frac{d(\mathbf{V}\cdot\mathbf{n})/dr}{\mathcal{H}}\right)\,. \tag{2.69}$$

In the last term we have converted d/dz into d/dr. For the volume perturbation this yields

$$V \;=\; \bar{V}+\delta V = \frac{r^2(z)}{(1+z)\mathcal{H}}\left(1+\mathbf{V}\cdot\mathbf{n}+\frac{d(\mathbf{V}\cdot\mathbf{n})/dr}{\mathcal{H}}\right)d\Omega_{\mathbf{n}}dz \tag{2.70}$$

$$\frac{\delta V}{V} \;=\; \mathbf{V}\cdot\mathbf{n}+\frac{d(\mathbf{V}\cdot\mathbf{n})/dr}{\mathcal{H}}\,. \tag{2.71}$$

At small to intermediate scales, the so called Doppler term $\mathbf{V}\cdot\mathbf{n}$ is usually neglected as it is a factor $\mathcal{H}/k$ smaller than the last term which contains an additional derivative.

Let us now consider a relatively small survey of galaxies positioned in a global direction $-\mathbf{n}$ from the observer and at observed redshift z. To take into account redshift space distortions (RSD) we have to take into account the radial volume distortion and replace the observed galaxy over density $\delta_g = b\delta$ by

$$\Delta = \frac{\delta N}{N} = \delta_g(\mathbf{x},z)+\frac{\delta V}{V} = b\delta(\mathbf{x},z)-\mathcal{H}^{-1}\mathbf{n}\cdot\nabla\left(\mathbf{n}\cdot\mathbf{V}(\mathbf{x},z)\right)\,, \tag{2.72}$$

where we have neglected the subdominant term of Eq. (2.71) and we assume the galaxy density fluctuation, δ_g, to be linearly related to the matter density fluctuation. We have inserted $\mathbf{x}=-r\mathbf{n}$ and we have used that $\partial_r = -\mathbf{n}\cdot\nabla$. The quantity b is a bias factor which depends on the chosen 'tracer' and is in general redshift dependent, but we assume it to be scale independent. We consider scalar perturbations such that $\mathbf{V}=-\nabla V_s$ for a velocity potential V_s. Fourier transforming Eq. (2.72) we find

$$\Delta(\mathbf{k},z) = b\delta(\mathbf{k},z)-\mu^2k^2V_s(\mathbf{k},z)/\mathcal{H}\,, \tag{2.73}$$

where $\mu=\hat{\mathbf{k}}\cdot\mathbf{n}$ is the direction cosine between the incoming photon and the wave number $\mathbf{k}$. We now use the Newtonian continuity equation in Fourier space,

$$\dot{\delta}+k^2V_s = 0\,. \tag{2.74}$$

We set $\delta(k,t) = D_1(t)\delta(k,t_0)$ where $D_1(t)$ is the deterministic linear growth factor which we normalize to 1 today. For pure matter perturbations D_1 does not depend on the wave number. We also introduce the logarithmic growth rate

$$f = \frac{\dot{D}_1}{D_1\mathcal{H}} \equiv \frac{d\ln D_1}{d\ln a}\,. \tag{2.75}$$

We then obtain for the observed power spectrum of Δ

$$P_{\rm obs}(\mathbf{k},z) = P_\delta(k,z)\left[b+\mu^2 f\right]^2 . \tag{2.76}$$

This is the very interesting result first derived by Kaiser [20]. It shows that even in a statistically isotropic universe the observed power spectrum is not isotropic due to observational effects. Furthermore, isolating the term proportional to μ^2 or μ^4 allows us to measure the growth function f which depends sensitively on the expansion history of the Universe.

The monopole term $b^2P_\delta(k,z)$ exhibits the so called Baryon Acoustic Oscillations 'BAOs' which are the acoustic oscillations of the baryon-photon fluid prior to decoupling left over in the baryons. Since baryons make only a small contribution to the total matter, the amplitude of BAO's is much smaller than the one of the acoustic oscillations in the CMB, but they have unambiguously been detected in the data and are routinely being used to measure a distance out to redshift z as follows:

Let us denote the comoving wavelength of the oscillations to be λ_n. In transversal directions they are seen under and angle $\theta_n(z) = \lambda_n/[(1+z)d_A(z)]$. In radial directions they are seen as a redshift difference $\Delta z_n = \lambda_n H(z)$. In an angular average the physical distance $d_V(z)$ which is estimated from these oscillations is given by

$$d_V(z) = \left(\frac{d_A^2(z)}{(1+z)H(z)}\right)^{1/3} . \tag{2.77}$$

If we can measure the radial and transversal BAO's independently, by determining Δz_n and θ_n in the angular power spectrum we can measure

$$F(z) \equiv \frac{\Delta z_n(z)}{(1+z)\theta_n(z)} = H(z)d_A(z) = H(z)\int_0^z \frac{dz'}{H(z')} . \tag{2.78}$$

This is the so called Alcock-Paczynski test [21] which we can perform whenever we can see the same physical scale, here λ_n, radially and transversally. Forecasts how well this can be measured in the angular correlation function with future surveys have been performed in the literature [22, 23]. At present, no experimental results are yet available.

One usually expands Eq. (2.76) in Legendre polynomials, which we denote here by L_ℓ (in order to avoid too many P's),

$$P_{\rm obs}(\mathbf{k},z) = P_\delta(k)D_1^2(z)\left[\beta_0(z)L_0(\mu)+\beta_2(z)L_2(\mu)+\beta_4(z)L_4(\mu)\right] \tag{2.79}$$

with

$$\beta_0 = b^2 + \frac{2bf}{3} + \frac{f^2}{5} \tag{2.80}$$

$$\beta_2 = \frac{4bf}{3} + \frac{4f^2}{7} \tag{2.81}$$

$$\beta_4 = \frac{8f^2}{35} . \tag{2.82}$$

$P_\delta(k)$ is the linear density fluctuation spectrum today.

The products $\beta_0P_\delta(k)$ and $\beta_2P_\delta(k)$ have been determined by observations at good accuracy, but $\beta_4P_\delta(k)$ has not yet been positively detected. Only when we are able to measure all three quantities, we will be able to break the degeneracy and isolate both b and f. In a ΛCDM or open universe $f(z) \simeq \Omega_m(z)^{0.55}$. For $\Omega_m(z=0) \sim 0.3$ we find that at low redshift $\beta_4 \sim 0.06$ while $\beta_0 \sim 4$ and $\beta_2 \sim 1.4$ for a typical bias factor $b \sim 2$. At higher redshift, $z \gtrsim 2$ we have $f \simeq 1$ so that $\beta_4(z \geq 2) \simeq 8/35 \simeq 0.23$. But unfortunately, presently there is no data available at these redshifts and as we shall see below, contributions from lensing cannot be neglected at $z = 2$ and larger.

Fourier transforming the power spectrum we obtain the correlation function,

$$\xi_{\rm obs}(\mathbf{d},z) = D_1^2(z)\left[\beta_0\xi_0(d)L_0(\mu) - \beta_2\xi_2(d)L_2(\mu) + \beta_4\xi_4(d)L_4(\mu)\right] . \tag{2.83}$$

where here μ denotes the direction cosine between the outward normal $\mathbf{n}$ and the vector $\mathbf{d}$ connecting the correlated galaxies and

$$\xi_n(d) = \int \frac{k^2dk}{2\pi^2} P_\delta(k) j_n(kd) . \tag{2.84}$$

The details of this are derived in Exercise 2.5.1. As we denote the comoving distance out to redshift z by $r(z)$, we here use $\mathbf{d}$ for the distance vector connecting the two 'pixels' which we correlate in ξ.

Lensing

In the previous section we considered radial volume distortions, in this section we consider transversal distortions due to lensing.

The observed transverse surface element is $\bar{r}^2 \sin\vartheta_o d\vartheta_o d\varphi_o$. The transverse surface element at emission, i.e. at the source, is $\bar{r}^2 \sin\vartheta_s d\vartheta_s d\varphi_s$.

Inserting $\vartheta_s = \vartheta_o + \delta\vartheta$, $\varphi_s = \varphi_o + \delta\varphi$, the ratio is to first order in the perturbations

$$\frac{\sin\vartheta_s}{\sin\vartheta_o}\left|\frac{\partial(\vartheta_s,\varphi_s)}{\partial(\vartheta_o,\varphi_o)}\right| = 1 + (\cot\vartheta_o + \partial_\vartheta)\delta\vartheta + \partial_\varphi\delta\varphi\,. \tag{2.85}$$

Here we used that $\det(\mathbb{1} + \epsilon M) = 1 + \epsilon\mathrm{Trace}M$ to first order in ϵ. Inserting $\delta\vartheta$ and $\delta\varphi$ from Eqs. (2.27) and (2.28), and using the definition of the lensing potential (2.5) we find

$$\begin{aligned}\frac{\sin\vartheta_s}{\sin\vartheta_o}\left|\frac{\partial(\vartheta_s,\varphi_s)}{\partial(\vartheta_o,\varphi_o)}\right| &= 1 - (\cot\vartheta_o\,\partial_\vartheta + \partial_\vartheta^2 + \frac{1}{\sin^2\vartheta_o}\partial_\varphi^2)\psi(\mathbf{n},z) &(2.86)\\ &= 1 - \Delta_\Omega\psi(\mathbf{n},z) \;=\; 1 - 2\kappa(\mathbf{n},z)\,. &(2.87)\end{aligned}$$

Here again Δ_Ω denotes the Laplacian on the 2-sphere w.r.t. the observed direction $-\mathbf{n} \equiv (\vartheta_o, \varphi_o)$. Adding also this transversal volume fluctuation we obtain

$$\Delta_{\rm obs}(\mathbf{x},z) = b\delta_z + \frac{\delta V}{V} = b\delta(\mathbf{x},z) - \mathcal{H}^{-1}\mathbf{n}\cdot\nabla\left(\mathbf{n}\cdot\mathbf{V}(\mathbf{x},z)\right) - 2\kappa(\mathbf{n},z)\,, \tag{2.88}$$

This is the correct result if we see all galaxies (of the type considered in a given survey). But a real telescope has a finite sensitivity and cannot see objects which emit light below a given flux limit F_* depending on the telescope. This flux limit is usually given in terms of a so called apparent magnitude limit,

$$m_* = -\frac{5}{2}\log_{10}F_* + \text{const.}\,, \tag{2.89}$$

where the constant is traditionally defined such that the star Vega has apparent magnitude zero. Note, the lower the magnitude of a galaxy the brighter it is. If galaxies are too faint, they are not observed in the given survey. However, due to the lensing magnification κ some galaxies which would be intrinsically too faint are amplified above the flux limit and make it into our survey. Denoting the mean number of galaxies with observed magnitude below m_*, flux higher than F_* or intrinsic luminosity above $L_*(z)$ by $\bar{n}_g(z, L_*)$, the observed number of galaxies below this magnitude in a given direction $-\mathbf{n}$ at redshift z is corrected by

$$n_g(z, L_*, \mathbf{n}) = \bar{n}_g(z, L_*) + \left.\frac{\partial\bar{n}(z,L)}{\partial\ln L}\right|_{L=L_*}\frac{\delta L}{L}\,. \tag{2.90}$$

Neglecting other relativistic effects apart from the focussing of light by lensing, we have $\delta L/L = \mu - 1 = 2\kappa$, see Eq. (2.7). Introducing the magnification bias

$$s(z, m_*) = \frac{2}{5}\left.\frac{\partial\bar{n}(z,L)}{\partial\ln L}\right|_{L=L_*(z)} \tag{2.91}$$

we obtain for the number counts

$$\begin{aligned}\Delta_{\rm obs}(\mathbf{n},z) &= b\delta_z + \frac{\delta V}{V} + \left.\frac{\partial\bar{n},L}{\partial\ln L}\right|_{L=L_*}\frac{\delta L}{L}\\ &= b\delta(r(z)\mathbf{n},z) - \mathcal{H}^{-1}\mathbf{n}\cdot\nabla\left(\mathbf{n}\cdot\mathbf{V}(r(z)\mathbf{n},z)\right) - (2-5s)\kappa(\mathbf{n},z)\,. &(2.92)\end{aligned}$$

The strange pre-factor in the definition of s comes from the fact that it was originally defined as a derivative w.r.t the apparent magnitude m_*.

This is the formula which includes RSD and the two effects of lensing. The increase of the transversal volume reduces the number count per volume element while the focussing enhances the number of galaxies that make it into a given survey. The two lensing terms therefore have opposite signs (as $\bar{n}_g(m)$ is monotonically growing with L, s is always positive, but not necessarily monotonic). Depending on the value of s one or the other term may dominate. At low redshift we usually see most galaxies and s is small. At high redshift however, we see only the brightest objects and s can become quite large. Depending on the survey, the pre-factor $(2-5s)$ can change sign at a given redshift. To take the lensing effect correctly into account we therefore have to measure $s(z)$ for the given survey. This can be done by choosing m_* slightly higher than the true limiting magnitude and counting $n_g(z, m_* - dm)$ and $n_g(z, m_* + dm)$.

As the lensing potential ψ it is given as an integral along the line of sight, the lensing term $\kappa(\mathbf{n},z) = \Delta\psi(\mathbf{n},z)$ in Eq. (2.92) does not simply depend on $\mathbf{x} = -r\mathbf{n}$. We can compute κ only on positions $\mathbf{x}$ which are on our background lightcone. Therefore, there is no simple, straight forward way to convert the expression (2.92) into a power spectrum in Fourier space for fixed $\mathbf{n}$ and z. It is much more natural to consider the redshift dependent correlation function or angular power spectrum of $\Delta_{\rm obs}(\mathbf{n},z)$.

$$\begin{aligned}\Delta_{\rm obs}(\mathbf{n},z) &= \sum_{\ell m} a_{\ell m}(z)Y_{\ell m}(n) &(2.93)\\ \langle a_{\ell m}(z)a^*_{\ell' m'}(z')\rangle &= C_\ell(z,z')\delta_{\ell\ell'}\delta_{m,m'} &(2.94)\\ \langle\Delta_{\rm obs}(\mathbf{n},z)\Delta_{\rm obs}(\mathbf{n}',z')\rangle &= \frac{1}{4\pi}\sum_\ell(2\ell+1)C_\ell(z,z')L_\ell(\mathbf{n}\cdot\mathbf{n}')\,. &(2.95)\end{aligned}$$

In Fig. 2.3 we show the power spectra including density, RSD and lensing for $z = z' = 1$ (top panel), $z = z' = 2$ middle panel and $z = 1, z' = 2$ lower panel. Interestingly for both, diagonal correlations the RSD contributions are larger than the density term. This is of course also due to our choice of $b = 1$ in the plot. Furthermore, the lensing term is negligible for the diagonal correlations. However, for $z = 1$ and $z' = 2$ the lensing term largely dominates the result and the density and RSD contributions are negligible. Of course this extreme case of an off-diagonal spectrum has a very low amplitude.

From the angular power spectrum which is well defined also for wide angle surveys, the growth function f cannot be readily extracted. Therefore, it is also very useful to measure the correlation function given in Eq. (2.83). For small angular separation we can define a common direction $\bar{\mathbf{n}}$ and split the distance $\mathbf{d} = r(z)\mathbf{n} - r(z')\mathbf{n}'$ into a radial and a transversal part, $\mathbf{d} = (r(z) - r(z'))\bar{\mathbf{n}} + \mathbf{d}_\perp$. For small redshift differences, $z = \bar{z} + \Delta z/2$, $z' = \bar{z} - \Delta z/2$, the correlation function can then be understood as a function of $d = |\mathbf{d}|$, $\mu = (r(z) - r(z'))/d$ and $\bar{z} = (z + z')/2$. As long as lensing can be neglected, the μ-dependence expressed in Legendre polynomials is proportional to the terms β_0, $-\beta_2$ and β_4. (When going from the power spectrum to the correlation function, the Legendre polynomial coefficients β_j which are not multiples of 4, $j \neq 4n$ acquire a minus sign due to the expansion of the exponential in Legendre polynomials and spherical Bessel functions, see Eq. (2.18) and Ex. 2.5.1. Furthermore, odd coefficients vanish if we consider only one population of galaxies.)

2.4.3 The fully relativistic angular matter power spectrum

Here we want to present the fully relativistic matter power spectrum. Its derivation is more involved as we take into account the full perturbed metric and also perturbations of the radial distance. Even though the final formula is significantly longer than Eq. (2.92), the new terms are only relevant at very large scales, $k/\mathcal{H} \sim 1$ as they are suppressed by at least one power of $\mathcal{H}/k$ w.r.t. the terms we have computed above. For typical surveys with redshifts up to $z \sim 3$ they can be safely neglected for $\ell > 20$. Nevertheless, we want to compute them here. First of all, if ever we can go to significantly higher redshifts, e.g. $z \sim 20$ or so for example with intensity mapping,

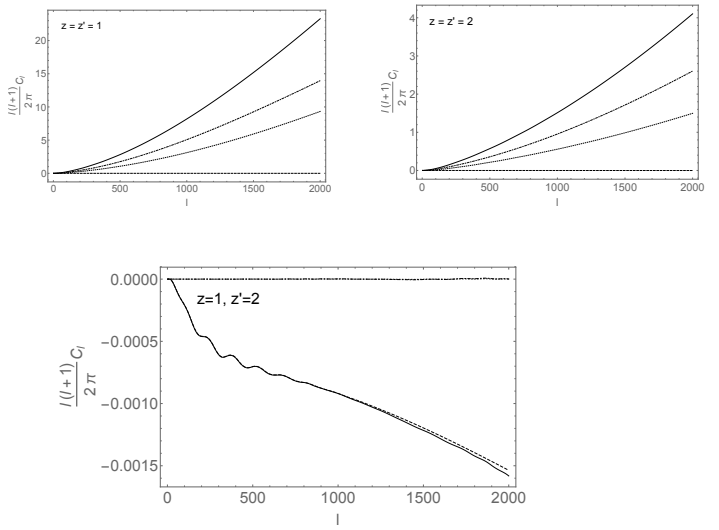

Figure 2.3: We show the observed matter angular power spectrum for $z = z' = 1$ (top left panel), $z = z' = 2$ (top right panel) and $z = 1, z' = 2$ (bottom panel). The solid line is the full result, the dotted line is the density term only, the dash-dotted line shows the RSD and RSD-density correlation and the dashed line show all terms containing κ. We have set $b = 1$ and $s = 0$.

these terms become relevant. Furthermore, they show how galaxy number counts are in principle sensitive not only to the density and velocity fields but also to metric perturbations. Therefore, they can be used to test the consistency of LSS with General Relativity. For this, we do not even need the large scale relativistic effects which we now determine; we can measure the lensing potential at sufficient redshift already with the dominant lensing term. Finally, the relativistic terms which we compute below, when converted to a power spectrum lead to an upturn of the power spectrum on very large scale exactly like the effect of a primordial non-Gaussianity as described in [24]. Therefore, neglecting it might lead to a false 'discovery' of primordial non-Gaussianity.

Let us start the fully relativistic derivation. We shall do the derivation in longitudinal (Newtonian) gauge. Since all multipoles with $\ell \geq 2$ vanish in the background they are gauge-invariant (Steward's lemma). The monopole and dipole however, are gauge dependent and we shall not consider them. For this reason we also disregard terms at the observer which contribute only to the monopole or the dipole. We present the derivation for vanishing spatial curvature. The expression for number counts in a spatially curved universe can be found in [25].

We first note that $\delta_z = \delta\rho/\bar{\rho}|_z$ i.e. the density fluctuation at fixed redshift is related to the density fluctuation at fixed time t by

$$\delta_z = \frac{\delta\rho}{\bar{\rho}} + \frac{d\bar{\rho}}{dz}\delta z = D_s - 3\frac{\delta z}{1+z}\,. \tag{2.96}$$

Here D_s is the matter density fluctuation in longitudinal gauge and δz is the redshift perturbation in longitudinal gauge given in Eq. (1.13). Let us also determine the relativistic volume perturbation. The 3-dimensional (spatial) volume element has to be defined w.r.t. an observer moving with 4-velocity u^μ as

$$\begin{aligned} dV &= \sqrt{-g}\epsilon_{\mu\nu\alpha\beta}u^\mu dx^\nu dx^\alpha dx^\beta \\ &= \sqrt{-g}\,\epsilon_{\mu\nu\alpha\beta}u^\mu \frac{\partial x^\nu}{\partial z}\frac{\partial x^\alpha}{\partial \vartheta_s}\frac{\partial x^\beta}{\partial \varphi_s}\left|\frac{\partial(\vartheta_s,\varphi_s)}{\partial(\vartheta_o,\varphi_o)}\right| dz d\vartheta_o d\varphi_o \\ &\equiv v(z,\vartheta_o,\varphi_o) dz d\Omega_o\,, \end{aligned} \tag{2.97}$$

where $d\Omega_o = \sin\vartheta_o d\vartheta_o d\varphi_o$, z is the source redshift, and we have introduced the density v which defines the volume perturbation,

$$\frac{\delta V}{V} = \frac{v-\bar{v}}{\bar{v}} = \frac{\delta v}{\bar{v}}.$$

As above, a suffix o denotes the observer position while a suffix s denotes the source (galaxy) position. In addition to the Jacobian of the transformation from the angles at the source to the angles at the observer, which we already had in the previous section, $\left|\frac{\partial(\vartheta_s,\varphi_s)}{\partial(\vartheta_o,\varphi_o)}\right|$, there are now terms coming from $\sqrt{-g}$ and the perturbations of the radial distance. Eq. (2.97) is still exact. To first order the perturbed angles at the source, $\vartheta_s = \vartheta_o + \delta\vartheta$ and $\varphi_s = \varphi_o + \delta\varphi$ have been determined in Eqs. (2.27) and (2.28). As in the previous section, at first order in the perturbations, the Jacobian determinant is

$$\left|\frac{\partial(\vartheta_s,\varphi_s)}{\partial(\vartheta_o,\varphi_o)}\right| = 1 + \frac{\partial\delta\vartheta}{\partial\vartheta} + \frac{\partial\delta\varphi}{\partial\varphi}. \tag{2.98}$$

Using the first order expression for the metric determinant, $\sqrt{-g} = a^4(1+\Psi-3\Phi)$ and the 4-velocity of the source, $(u^\mu) = \frac{1}{a}(1-\Psi, V^i)$, we find to first order

$$v = a^3(1+\Psi-3\Phi)\left[\frac{dr}{dz}r^2\frac{\sin\vartheta_s}{\sin\vartheta_o}\left(1+\frac{\partial\delta\vartheta}{\partial\vartheta}+\frac{\partial\delta\varphi}{\partial\varphi}\right)(1-\Psi+V_r)\right]. \tag{2.99}$$

Here dr/dz is to be understood as the derivative of the comoving distance r with respect to the redshift along the photon geodesic. At linear order we can write (the distinction between the true z and and the background $\bar{z}$ is only relevant for background quantities)

$$\frac{dr}{dz} = \frac{d\bar{r}}{d\bar{z}} + \frac{d\delta r}{d\bar{z}} - \frac{d\delta z}{d\bar{z}}\frac{d\bar{r}}{d\bar{z}} = \left(\frac{d\bar{r}}{dt} + \frac{d\delta r}{d\lambda} - \frac{d\delta z}{d\lambda}\frac{d\bar{r}}{d\bar{z}}\right)\frac{dt}{d\bar{z}}, \tag{2.100}$$

where we have used that for first order quantities we can set $dt = d\lambda$ when we have to take the derivative along the photon geodesic. The last term of Eq. (2.100) contains the redshift space distortion discussed in the previous section. To lowest order along a photon geodesic $-d\bar{r}/d\bar{z} = dt/d\bar{z} = -H^{-1} = -a/\mathcal{H}$. With this the volume element becomes

$$v = \frac{a^4\bar{r}^2}{\mathcal{H}}\left[1 - 3\Phi + \left(\cot\vartheta_o + \frac{1}{\partial\vartheta}\right)\delta\vartheta + \frac{\partial\delta\varphi}{\partial\varphi} - \mathbf{V}\cdot\mathbf{n} + \frac{2\delta r}{r} - \frac{d\delta r}{d\lambda} + \frac{a}{\mathcal{H}}\frac{d\delta z}{d\lambda}\right]. \tag{2.101}$$

From this we subtract the unperturbed part $\bar{v}(z)$ evaluated at the observed redshift, $z = \bar{z} + \delta z$,

$$\bar{v}(z) = \bar{v}(\bar{z}) + \frac{d\bar{v}}{d\bar{z}}\delta z.$$

With the unperturbed expression, $a = 1/(\bar{z}+1)$,

$$\bar{v}(\bar{z}) = \frac{\bar{r}^2}{(1+\bar{z})^4\mathcal{H}} \tag{2.102}$$

we obtain

$$\begin{aligned}\frac{\delta v}{\bar{v}}(\mathbf{n},z) &= \frac{v(z)-\bar{v}(z)}{\bar{v}(z)} \\ &= -3\Phi + \left(\cot\vartheta_o + \frac{\partial}{\partial\vartheta}\right)\delta\vartheta + \frac{\partial\delta\varphi}{\partial\varphi} - \mathbf{V}\cdot\mathbf{n} + \frac{2\delta r}{r} - \\ &\quad \frac{d\delta r}{d\lambda} + \frac{1}{\mathcal{H}(1+\bar{z})}\frac{d\delta z}{d\lambda} - \left(-4 + \frac{2}{\bar{r}\mathcal{H}} + \frac{\dot{\mathcal{H}}}{\mathcal{H}^2}\right)\frac{\delta z}{1+\bar{z}}. \end{aligned} \tag{2.103}$$

To compute the radial perturbation δr we have to integrate the photon geodesic from the source to the observer. We use

$$\frac{dx^\mu}{d\lambda} = n^\mu\,, \tag{2.104}$$

where n^μ denotes the photon four velocity. Neglecting perturbations at the observer position which give raise to unobservable monopole and dipole terms, using Eqs. (1.10) and (1.11) we find

$$\delta x^i(t_s) = -2\int_0^{r_s} dr(\Psi+\Phi)\mathbf{n}^i - \int_0^{r_s} dr(r_s-r)\Big((\Psi+\Phi)_{,i} + (\dot{\Psi}+\dot{\Phi})\mathbf{n}^i\Big), \tag{2.105}$$

where we have used $r_s - r(\lambda) = \lambda$ and $dr = -d\lambda$ to lowest order. From this we obtain

$$\delta r \equiv \delta x^i n_{ri} = \int_0^{r_s} dr(\Phi+\Psi)\,. \tag{2.106}$$

We have also used that $\mathbf{n} = -\mathbf{n}_r$, $\mathbf{n}^i\partial_i + \partial_t = \frac{d}{d\lambda} = \frac{d}{dt}$ and $r_s = t_0 - t_s$ to lowest order. For the derivative of δr we obtain

$$\frac{d\delta r}{d\lambda} = -(\Phi+\Psi). \tag{2.107}$$

Inserting Eqs. (2.27) and (2.28) for the angular contribution to the volume we find as in the previous section

$$\begin{aligned}(\cot\vartheta + \partial_\vartheta)\delta\vartheta + \partial_\varphi\delta\varphi &= -\int_0^{r_s} dr\frac{(r_s-r)}{rr_s}\Delta_\Omega(\Phi+\Psi) \\ &= -\int_0^{r_s} dr\frac{(r_s-r)r}{r_s}\Delta_\perp(\Phi+\Psi) = -2\kappa \end{aligned} \tag{2.108}$$

where Δ_Ω denotes the angular part of the Laplacian and $\Delta_\perp \equiv r^{-2}\Delta_\Omega$,

$$\Delta_\Omega \equiv \left(\cot\vartheta\partial_\vartheta + \partial_\vartheta^2 + \frac{1}{\sin^2\vartheta}\partial_\varphi^2\right). \tag{2.109}$$

Adding all the contributions of Eq. (2.103) together we obtain

$$\begin{aligned}\frac{\delta v}{v} &= -2(\Psi+\Phi) - 4\mathbf{V}\cdot\mathbf{n} + \frac{1}{\mathcal{H}}\left[\dot{\Phi} + \partial_r\Psi - \frac{d(\mathbf{V}\cdot\mathbf{n})}{d\lambda}\right] \\ &\quad + \left(\frac{\dot{\mathcal{H}}}{\mathcal{H}^2} + \frac{2}{r_s\mathcal{H}}\right)\left(\Psi + \mathbf{V}\cdot\mathbf{n} + \int_0^{r_s} dr(\dot{\Phi}+\dot{\Psi})\right) \\ &\quad -3\int_0^{r_s} dr(\dot{\Phi}+\dot{\Psi}) + \frac{2}{r_s}\int_0^{r_s} dr(\Phi+\Psi) - \frac{1}{r_s}\int_0^{r_s} dr\frac{r_s-r}{r}\Delta_\Omega(\Phi+\Psi). \end{aligned} \tag{2.110}$$

Adding this to the density perturbation in redshift space given in Eq. (2.96), we obtain the number count fluctuations to first order [26],

$$\begin{aligned}\Delta(\mathbf{n},z) &= D_s - 2\Phi + \Psi + \frac{1}{\mathcal{H}}\left[\dot{\Phi} + \partial_r(\mathbf{V}\cdot\mathbf{n})\right] \\ &\quad + \left(\frac{\dot{\mathcal{H}}}{\mathcal{H}^2} + \frac{2}{r_s\mathcal{H}}\right)\left(\Psi + \mathbf{V}\cdot\mathbf{n} + \int_0^{r_s} dr(\dot{\Phi}+\dot{\Psi}\right) \\ &\quad + \frac{1}{r_s}\int_0^{r_s} dr\left[2 - \frac{r_s-r}{r}\Delta_\Omega\right](\Phi+\Psi)\,. \end{aligned} \tag{2.111}$$

Here we have also used the momentum conservation equation for pressureless matter,

$$\mathbf{n}\cdot\dot{\mathbf{V}} + \mathcal{H}\mathbf{n}\cdot\mathbf{V} - \partial_r\Psi = 0\,,$$

in order to remove the term $\dot{\mathbf{V}}$ in $d\mathbf{V}/d\lambda = \dot{\mathbf{V}} + n^i\partial_i\mathbf{V}$. The terms in the integrals have always to be evaluated at the positions $\mathbf{x} = -r\mathbf{n}, t = t_0 - r$, while the source position is $\mathbf{x}_s = -r_s\mathbf{n}, t_s = t_0 - r_s$ and we set $\mathbf{x}_o \equiv 0$.

This is the observable linear matter density fluctuation in angular and redshift space. Note, that we did not use Einstein's equation in this derivation which is therefore valid for all metric theories of gravity, i.e. theories where photons and dark matter particles move along geodesics.

As we have already seen, the last term of Eq. (2.111) is simply the convergence κ, i.e. the trace of the Jacobian of the lens map, which we have already obtained in the previous section,

$$-2\kappa = -\Delta_\Omega\psi = -\Delta_\Omega\int_0^{r_s} dr\frac{r_s-r}{r_s r}(\Phi+\Psi)\,. \tag{2.112}$$

As already discussed, galaxies are biased tracers of the matter density fluctuations. In relativistic perturbation theory there are different gauge-invaiant definitions of the matter density fluctuation, and we have to decide which one might be linearly related to the galaxy density. It is physically most sensible to assume that a linear relation exists between the matter density and the galaxy density in *comoving gauge*, i.e. in the gauge where matter is at rest. The matter density in this gauge is D which is related to the density D_s in longitudinal gauge by

$$D = D_s - \frac{\dot{\rho}}{\rho} V = D_s + 3\mathcal{H}V_s \,, \tag{2.113}$$

where V_s is the velocity potential introduced in the previous section, $\mathbf{V} = -\nabla V_s$. (Note that V_s in real space defined in this way has the dimension of a length. It is related to the dimensionless V in Fourier space defined via $V(k) = kV_s(k)$). We assume that in comoving gauge the galaxy number density fluctuation is proportional to the matter density fluctuation,

$$\delta_g = bD \,, \tag{2.114}$$

where b is a bias factor which generically depends on redshift. Bias can also be more complicated, scale-dependent, non-linear, stochastic etc., but we do not consider these possibilities in our discussion.

Furthermore, the comoving galaxy number density may increase due to the formation of new galaxies (or decrease due to mergers), so that the physical number density of galaxies decays slower (or faster) than the mean matter density. We model this as

$$\dot{N}/N = (1 - b_e/3)\dot{\rho}/\rho \,, \tag{2.115}$$

where b_e is called 'evolution bias'. Therefore we have to replace D_s not simply by $bD - 3\mathcal{H}V_s$ but by

$$D_s^{\rm obs} = bD - (3 - b_e)\mathcal{H}V_s \,. \tag{2.116}$$

In addition, in Eq. (2.96) we have used that $d\bar{\rho}_m/dz = -3\bar{\rho}_m/(1+z)$. If galaxies are generated as modelled with the evolution bias b_e in Eq. (2.115), we have to replace the term $-3\delta z/(1+z)$ by $(-3+b_e)\delta z/(1+z)$. This adds a term $-b_e$ in the parenthesis $(\dot{\mathcal{H}}/\mathcal{H}^2 + 2/(r_s\mathcal{H}))$ of Eq. (2.111).

Finally, we also want to take into account magnification bias. As in the previous section, the number count fluctuations up to a limiting flux F_* are given by

$$\Delta_g(\mathbf{n}, z, m_*) = \Delta_g(\mathbf{n}, z) + \left.\frac{\partial \ln \bar{n}_g(z, L)}{\partial \ln L}\right|_{L=L_*} \frac{\delta L}{\bar{L}} = \Delta_g(\mathbf{n}, z) + \frac{5s}{2}\frac{\delta L}{\bar{L}} \,, \tag{2.117}$$

where s is as defined in Eq. (2.91). In a relativistic treatment we have to be more careful in the determination of the luminosity perturbation. In terms of the fluctuation of the luminosity distance it is given by $\delta L/\bar{L} = -2\delta D_L/\bar{D}_L$. In Section 2.3 we have calculated the perturbation of the luminosity distance. Inserting the result given in Eq. (2.62) and putting all the biasing effects together, we find [27]

$$\begin{aligned}\Delta_g(\mathbf{n}, z, m_*) \;=\; & bD - (3 - b_e)\mathcal{H}V + \frac{1}{\mathcal{H}}\left[\dot{\Phi} + \partial_r(\mathbf{V}\cdot\mathbf{n})\right] + \\ & \left(\frac{\dot{\mathcal{H}}}{\mathcal{H}^2} + \frac{2-5s}{r_s\mathcal{H}} + 5s - b_e\right)\left(\Psi + \mathbf{V}\cdot\mathbf{n} + \int_0^{r_s} dr(\dot{\Phi} + \dot{\Psi})\right) \\ & -(2-5s)\Phi + \Psi + \frac{2-5s}{2r_s}\int_0^{r_s} dr\left[2 - \frac{r_s - r}{r}\Delta_\Omega\right](\Phi + \Psi) \,,\end{aligned} \tag{2.118}$$

Like in Eq. (2.92), also in Eq. (2.118) s enters mainly in the combination $2-5s$. The first term is a transversal volume distortion. Focussing increases the angular separation of two points at a given transverse distance and hence lets the volume appear larger and the density smaller. On the other hand, focussing also enhances the luminosity of sources and galaxies which otherwise would be too faint to make it into our surveys, leading to an enhanced density. Depending on the sign of $2-5s$ one or the other effect wins. As we shall see in Section 2.5, for intensity maps the two effects exactly cancel. If we do not count individual sources but the intensity coming from a certain area, the area 'appears' larger due to focussing exactly by the increase in the luminosity coming from it so that the surface brightness is conserved. Therefore for intensity mapping we can simply set $s = 2/5$ and there is no lensing effect at first order in perturbation theory. This is also the case for CMB observations where lensing is a pure second order effect.

Let us now compute the relativistic angular matter power spectrum for the case of purely scalar adiabatic fluctuations. We assume that the initial fluctuations are given in Fourier space by the initial curvature fluctuation

$\zeta(\mathbf{k})$ given by

$$\zeta = \frac{2}{3(1+w)}\left[\Psi + \mathcal{H}^{-1}\dot{\Phi}\right] + \Phi \simeq \frac{5}{3}\Psi\,. \tag{2.119}$$

which has been generated during inflation with some power spectrum

$$k^3\langle\zeta(\mathbf{k})\zeta^*(\mathbf{k}')\rangle = (2\pi)^3\delta^3(\mathbf{k}-\mathbf{k}')\mathcal{P}_\zeta(k)\,. \tag{2.120}$$

The star indicates complex conjugation.

In the simplest models of adiabatic perturbations all scalar perturbations at later times are determined by the random variable $\zeta(\mathbf{k})$ via a deterministic transfer function,

$$X(\mathbf{k},z) \;=\; T_X(k,z)\zeta(\mathbf{k})\,, \qquad \mathbf{V}(\mathbf{k},z) \;=\; i\hat{\mathbf{k}}T_V(k,z)\zeta(\mathbf{k})\,. \tag{2.121}$$

The first equation applies for scalar quantities while the second one applies for (spatial) vectors, $\hat{\mathbf{k}}$ is the unit vector in direction $\mathbf{k}$. Note that within first order perturbation theory, z in these perturbation variables can be related to t via the background Friedmann model. In Fourier space therefore the vector $\mathbf{V} = i\hat{\mathbf{k}}V$ and the potential V have the same dimension. (As already mentioned, the Fourier transform of the velocity potential $V_s(\mathbf{x})$ is not $V(\mathbf{k})$ but $k^{-1}V(\mathbf{k})$.) The transfer functions depend on the content of the Universe and on the theory of gravity. Therefore, like for the CMB, measuring the galaxy power spectrum under the assumption of simple initial conditions, allows us to measure cosmological parameters.

To determine the number count power spectrum $C_\ell(z,z')$ and the angular correlation function

$$\xi(\theta,z,z') = \frac{1}{4\pi}\sum_\ell (2\ell+1)C_\ell(z,z')L_\ell(\cos\theta)\,, \tag{2.122}$$

we make again use of the identity

$$\exp(i\mathbf{k}\cdot\mathbf{r}) = \sum_\ell i^\ell j_\ell(kr)L_\ell(\hat{\mathbf{k}}\cdot\hat{\mathbf{r}})\,. \tag{2.123}$$

A short calculation using Eq. (2.118) gives (see [26])

$$C_\ell(z,z') = \frac{2}{\pi}\int\frac{dk}{k}\mathcal{P}_\zeta(k)F_\ell(k,z)F_\ell(k,z'), \tag{2.124}$$

where, $r_s \equiv r(z) = t_0 - t(z)$ is the comoving distance of the source and

$$\begin{aligned} F_\ell(k,z) \;=\; & j_\ell(kr_s)\Bigg[bT_D - (3-b_e)\frac{\mathcal{H}}{k}T_V + (2-5s)T_\Phi + \frac{1}{\mathcal{H}}\dot{T}_\Phi \\ & + \left(1 - \frac{\dot{\mathcal{H}}}{\mathcal{H}^2} + \frac{2-5s}{r_s\mathcal{H}} + 5s - b_e\right)T_\Psi\Bigg] \\ & + j_\ell'(kr_s)\left(\frac{\dot{\mathcal{H}}}{\mathcal{H}^2} + \frac{2-5s}{r_s\mathcal{H}} + 5s - b_e\right)T_V + \frac{k}{\mathcal{H}}T_V j_\ell''(kr_s) \\ & + \frac{2-5s}{2r_s}\int_0^{r_s} j_\ell(kr)\left(2 + \frac{r_s - r}{r}\ell(\ell+1)\right)(T_\Psi + T_\Phi)dr \\ & + \left(\frac{\dot{\mathcal{H}}}{\mathcal{H}^2} + \frac{2-5s}{r_s\mathcal{H}} + 5s - b_e\right)\int_0^{r_s} j_\ell(kr)(\dot{T}_\Psi + \dot{T}_\Phi)dr\,. \end{aligned} \tag{2.125}$$

The prime in the spherical Bessel functions denotes the derivative w.r.t. the argument. Let us briefly estimate the order of magnitude of the different terms in a standard ΛCDM cosmology. Neglecting anisotropic stresses and using the perturbed Einstein equations, it is easy to express all the transfer functions in terms of T_Ψ,

$$T_\Phi \;=\; T_\Psi \tag{2.126}$$

$$T_D \;=\; -\frac{2a}{3\Omega_m}\left(\frac{k}{\mathcal{H}_0}\right)^2 T_\Psi \tag{2.127}$$

$$\frac{k}{\mathcal{H}}T_V \;=\; \frac{2a}{3\Omega_m}\left(\frac{k}{\mathcal{H}_0}\right)^2\left(T_\Psi + \frac{\dot{T}_\Psi}{\mathcal{H}}\right) \tag{2.128}$$

Here $\mathcal{H}_0 = H_0$ is the present Hubble parameter and Ω_m is the present matter density parameter. On scales $k \gg \mathcal{H}_0$ the density term, $\propto (k/\mathcal{H}_0)^2 T_\Psi$ and the RSD term $\propto (k/\mathcal{H})T_V \propto (k/\mathcal{H}_0)^2 T_\Psi + \cdots$ clearly dominate (the $\cdots$ denote additional subdominant contributions). Furthermore, considering that for source redshift of order unity and more, $r_s \sim \mathcal{H}_0^{-1}$, so that a given angular scale $\ell \simeq \pi/\theta \simeq kr_s \simeq k/\mathcal{H}_0$, we find that for sufficiently high redshifts, $z \gtrsim 1$, also the κ-contribution to the lensing term is of the same order. However, when applying the Limber approximation, see [14, 15], to the lensing integrals, one finds that the integral removes one factor of ℓ from the result so that the first two terms are dominant for correlations at equal redshifts,

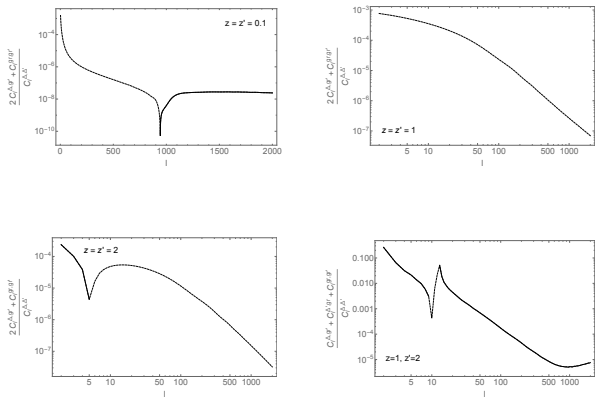

Figure 2.4: The large scale relativistic corrections to the power spectrum from the gravitational potential terms are shown for $z = z' = 0.1$ (top, left panel), $z = z' = 1$ (top, right panel), $z = z' = 2$ (bottom, left panel) and $z = 1, z' = 2$ (bottom, right panel). The dashed lines show negative contributions (in log scale). The contributions are always significantly less than 1% except at very low ℓ in the case $1 = z \neq z' = 2$.

$z = z'$. The RSD is the dominant radial volume distortion while the lensing or magnification term $\propto \kappa$ is the dominant transversal volume distortion.

When the redshift difference is substantial or when a wide redshift window is used, the lensing term cannot only become of the same order but it can even dominate over the standard density and RSD terms (see [28]). The remaining gravitational potential and Doppler terms are relevant only on very large scales and special techniques like multi tracer methods are required to render them observable (see, e.g., [29, 30]).

The terms multiplied by $2-5s$ all appear also in relativistic weak lensing expressions, in the perturbation of the determinant of the magnification matrix given in Eq. (2.6). The term $(2/r_s)\int_0^{r_s}(\Phi+\Psi)dr$ is the Shapiro time delay

coming from the prolongation of the photon path when it passes through a potential well. In addition to this there are the integrated Sachs Wolfe term (ISW), the Doppler term and the value of the gravitational potential at the source, see also Section 2.3.

Contrary to the density fluctuation $D(\mathbf{x}, t)$ the observable number count fluctuations $\mathbf{\Delta}(\mathbf{n}, z)$ also have contributions from vector and tensor fluctuations. We do not derive these here. They can be found in the literature e.g. the power spectrum $C_\ell(z, z')$ from tensor fluctuations is derived in [26] while the one for vector perturbation is given in [31].

In Fig. 2.4 we show the large scale relativistic corrections to the $C_\ell(z, z')$ power spectra. For $z = z'$ these never exceed a fraction of 10^{-3} of the total result for the redshifts $z = 1$ and $z = 2$ chosen here. For low redshifts, $z \simeq 0.1$ the relativistic contributions are much larger as we shall see when considering the correlation function. Here we have chosen a delta function window, or perfect resolution, in redshift. Smoothing over a wider redshift window can significantly enhance the fractional contribution of the relativistic terms as it reduces the density and RSD contributions. Also for $z \neq z'$, see bottom right panel of Fig. 2.4, the relativistic terms can make up to 20% on large scales.

At present, observers have not yet determined the angular power spectrum of number counts. So far they mainly used the flat sky approximation and determined the power spectrum from a small-angle patch of the sky or the correlation function which we discuss in the next section.

2.4.4 The correlation function

The observable angular-redshift power spectrum $C_\ell(z, z')$ is routinely calculated with fast codes as we have them for the CMB angular power spectrum. The presently most popular CMB codes CAMB and CLASS have been extended to compute also these spectra, see [27] and [32]. This is very useful as these spectra contain all the observable information. However, to compute only the C_ℓ's is not really optimal for spectroscopic redshift surveys. These surveys can observe tens of millions of galaxies with a redshift resolution of about $\delta z = 10^{-3}$ over a redshift interval $z \in [0.5, 2.5]$ this amounts to about 2000 redshift bins. The full computation of all possible $C_\ell(z, z')$ therefore comprises more than a million spectra. When using angular power spectra to estimate cosmological parameters we proceed via the Markov-Chain Monte-Carlo technique which requires the computation of about 10^5 spectra

per chain. For the number counts this would be equivalent to 10^{11} CMB spectra which is simply forbidding even if highly parallelized.

Furthermore, with 1000 bins there are only about 10^3 to 10^4 galaxies per bin which implies significant 'shot noise'. $C_\ell(z,z')$ is a function of 3 variables which is much harder to determine by observations than a simple power spectrum $P_\delta(k)$ or, including RSD, $\beta_0 P_\delta(k)$ together with β_2/β_0 and β_4/β_0. Therefore, shot noise, i.e. the fact that we have a finite number of galaxies to probe this function, is usually the limiting factor especially for high ℓ's.

As we have seen in the previous section, beyond $\ell \sim 20$ only three terms are really important: the density, redshift space distortions and the lensing term. Furthermore, density and RSD generate only a monopole, quadrupole ($n = 2$) and hexadecapole ($n = 4$) in the correlation function. The lensing, however also generates higher (even) multipoles. As we have seen in Section 2.4.2, if RSD is the dominating contribution to the quadrupole ($n = 2$) and hexadecapole ($n = 4$), their measurements can be used to isolate the bias and the growth function.

We shall see below, that for close redshifts, $|z - z'| \ll 1$, we can define a fully relativistic correlation function which in the limit of small d and small redshifts reduces to the one determined in Section 2.4.2. We first introduce the angular correlation function,

$$\xi(\theta, z, z') = \frac{1}{4\pi}\sum_\ell (2\ell+1) C_\ell(z,z') L_\ell(\cos\theta)\,. \tag{2.129}$$

Using the cosine law, the distance d between the two pixels which we correlate is given by ($r = r(z)$, $r' = r(z')$)

$$d = \sqrt{r^2 + r'^2 - 2rr'\cos\theta}\,. \tag{2.130}$$

Note that the value $r(z)$ depends on the cosmological parameters. Only for very small z we have $r(z) = H_0^{-1} z$, and we can absorb the dependence of r on H_0 by measuring distances in units of h^{-1}Mpc. For redshifts of order unity and more, $r(z)$ depends also on Ω_m, Ω_Λ and on the curvature Ω_K (which is neglected in expression (2.130).

We introduce also

$$\mu = \frac{r - r'}{d} = \frac{d_\parallel}{d} \qquad \text{and} \qquad d_\perp = \sqrt{d^2 - d_\parallel^2}\,. \tag{2.131}$$

Elementary geometry shows (exercise!) that this is the cosine of the angle α in Fig. 2.5. The definition of μ requires the measurement of θ, z, z' and the

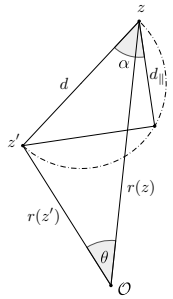

Figure 2.5: The variable μ is the cosine of the angle α between the line of length $d_\parallel$ which intersects the Thales circle over d and d itself.

choice of a cosmology which determines $r(z)$, $r(z')$ and via Eq. (2.130) also d. So far, observers have used a somewhat different definitions of μ, e.g. the angle between the vector $\mathbf{d}$ and the radial line dividing the angle θ or the one dividing d, but the results are very similar for most choices.

Setting $\bar z = (z + z')/2$ and $\Delta z = (z - z')/2$ we have $\Delta r = (r - r')/2 = \mathcal{H}(\bar z)^{-1}\Delta z + \mathcal{O}(\Delta z^2)$, hence $\Delta z = \mu d\mathcal{H}(\bar z)/2$ and

$$z = \bar z + \mu d\mathcal{H}(\bar z)/2 \tag{2.132}$$

$$z' = \bar z - \mu d\mathcal{H}(\bar z)/2 \tag{2.133}$$

$$\cos\theta = \sqrt{\frac{r^2 + r'^2 - d^2}{2rr'}} = \left(\frac{2\bar r^2 - d^2 + \frac{1}{2}\mu^2 d^2}{2\bar r^2 - \frac{1}{2}\mu^2 d^2}\right)^{1/2} \tag{2.134}$$

$$= \left(\frac{2\bar r^2 - d_\perp^2 - \frac{1}{2}d_\parallel^2}{2\bar r^2 - \frac{1}{2}d_\parallel^2}\right)^{1/2} \equiv c(\bar z, d, \mu)\,. \tag{2.135}$$

With this we can now write the correlation function as function of the separation d, the direction cosine μ and the mean redshift $\bar z$,

$$\xi(d, \mu, \bar z) = \frac{1}{4\pi}\sum_\ell (2\ell+1) C_\ell(z,z') L_\ell\left(c(\bar z, d, \mu)\right)\,, \tag{2.136}$$

where c is given in Eq. (2.135) and $z,\ z'$ in Eqs. (2.132) and (2.133). This form is valid only for $|z - z'| \ll 1$ at first order in $|z - z'|$. Alternatively, we may express $\cos\theta$ as function of $z,\ z'$ and d using Eq. (2.134) to obtain $\xi(d, z, z')$ which is valid also for large redshift differences $|z - z'|$.

It is important to always keep in mind that the step from the angular to the distance correlation function requires the assumption of a cosmological model. Contrary to $\xi(\theta, z, z')$, the correlation function $\xi(d, \mu, \bar{z})$ or $\xi(d, z, z')$ is model dependent. When using it to constrain cosmological parameters this has to be taken into account.

The advantage of the correlation function $\xi(d, \mu, \bar{z})$ w.r.t. the angular power spectrum is that in the small scale, small redshift, small angle limit it reduces to the non-relativistic expression (2.83). We can therefore use it in this limit to determine the growth function f and the bias b directly from its quadrupole and hexadecapole. Of course this information is also contained in the angular power spectrum, but there it is mixed together with other parameters. Another advantage of the correlation function is that within a sizable redshift bin $[\bar{z} - \Delta z, \bar{z} + \Delta z]$ we can expect to find many galaxies with separation in a small bin around d and around μ so that for many values of d and μ shot noise is not a serious problem.

In Fig. 2.6 we plot the correlation function as a function of d for fixed $\mu = 0.95$ at redshifts $\bar{z} = 0.1$, $\bar{z} = 1$ and $\bar{z} = 2$. The solid line includes all the terms, the dashed line includes only the 'standard terms', density and redshift space distortions while the dotted line includes also the lensing term. The difference between the full result and the density +RSD+lensing terms is nearly invisible for $z = 1$ and $z = 2$, while for $z = 0.1$ the lensing term is negligible (the dashed and the dotted lines nearly overlay) but the large scale relativistic corrections are clearly visible. These are the terms which contain a factor $1/r(z)$ (especially the Doppler term) which is much larger than $\mathcal{H}(z)$ at low redshift. These terms are then suppressed only by a factor $(d/r(z))^2 \gg (d\mathcal{H}(z))^2$ in the correlation function. For small values of μ, the lensing is of course much less relevant as is clear from Fig. 2.7. The pronounced feature at $d \simeq 100h^{-1}$Mpc is the BAO peak. Its position is quite stable under non-linearities but depends very sensitively on cosmological parameters. It is therefore routinely used to estimate the distance out to a given redshift z. While the relativistic terms make the correlation function at $z = 0.1$ more negative at large distance, the lensing terms contributes positively so that for $z = 2$ the correlation function even becomes positive again at $d \simeq 380h^{-1}$Mpc.

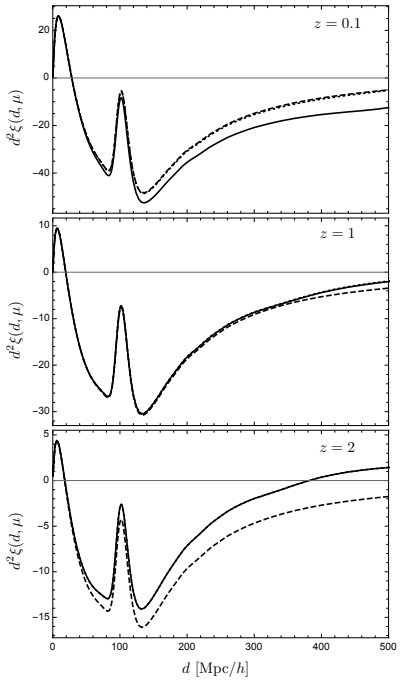

Figure 2.6: The correlation function is shown at redshifts $\bar{z} = 0.1$ (top panel), $\bar{z} = 1$ (middle panel) and $\bar{z} = 2$ (bottom panel) as a function of d for $\mu = 0.95$. The solid lines are the full result, the dashed lines include only the standard terms (density and RSD) and the dotted lines include also the lensing term.

In Fig. 2.7 the correlation function is shown at fixed $d = 350h^{-1}$Mpc as function of μ. In forward direction, $\mu \sim 1$, for redshifts $z = 1$ and 2 the

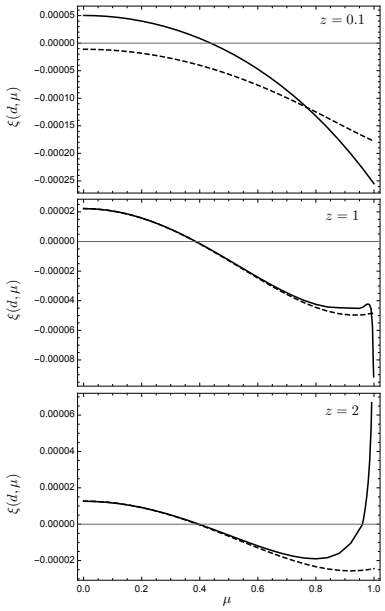

Figure 2.7: The correlation function is shown at redshifts $\bar{z} = 0.1$ (top panel) $\bar{z} = 1$ (middle panel) and $\bar{z} = 2$ (bottom panel) as a function of μ for $d = 350h^{-1}$Mpc. The solid lines are the full result, the dashed lines include only the standard terms.

lensing term is very important, even dominant, while for $\mu < 0.6$ it becomes irrelevant. For $\mu \to 1$, the lensing contribution is negative at $z = 1$ while it is positive at $z = 2$. This is due to the fact that at low redshift, $z \lesssim 1.5$ the negative cross term $D \cdot \kappa$ dominates while at higher redshift the positive $\kappa \cdot \kappa$ term dominates. The significant difference of the standard terms from the

relativistic expression at very low redshift, $z = 0.1$ comes from the Doppler term, which at $d = 350h^{-1}$Mpc dominates the signal.

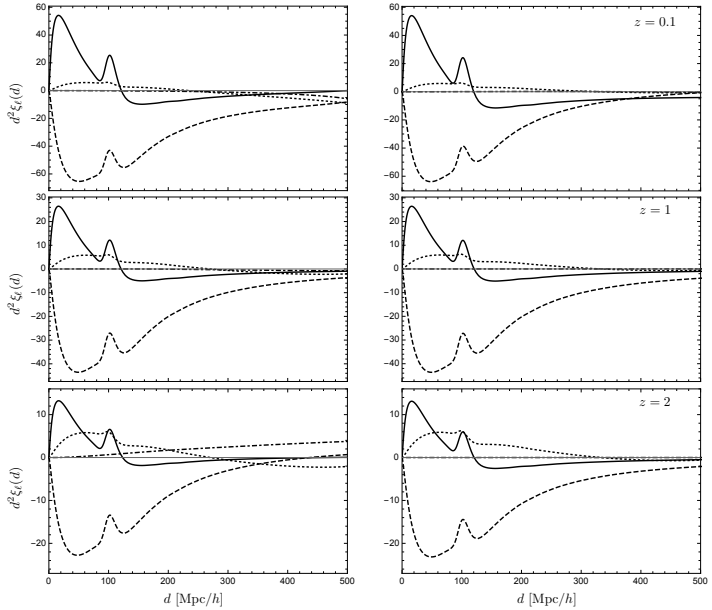

Figure 2.8: The correlation function multipoles $n = 0$ (solid), $n = 2$ (dashed), $n = 4$ (dotted) and $n = 6$ (dot-dashed) are shown at redshifts $\bar{z} = 0.1$ (top, left panel), $\bar{z} = 1$ (middle left panel) and $\bar{z} = 2$ (bottom, left panel) as a function of d. For comparison we plot the standard multipoles (density and RSD) in the right panels. Note that on very large scales, for $z = 0.1$ and for $z = 2$ the multipole $n = 6$ is comparable in amplitude to $n = 4$ on large scales.

In Fig. 2.8 we plot the multipoles of the correlation function with (left panels) and without (right panels) the lensing and large scale relativistic terms. The standard terms only generate $n = 0,\ 2$ and 4 multipoles, while lensing and other integrated relativistic terms also lead to higher multipoles. Especially at $z = 2$, the $n = 6$ multipole which comes from lensing is of the same order as the hexadecupole ($n = 4$). At large scales, $d > 200h^{-1}$Mpc it is even larger. Clearly, ignoring the lensing term produces very significant errors in the multipoles which cannot be tolerated in the analysis of future galaxy surveys.

In the monopole and the quadrupole of the correlation function the BAO peak is again very pronounced. Note also, that including relativistic effects, the monopole becomes positive again at very large scales while considering the standard terms only, it remains negative. The same is true for the quadrupole at $z = 2$. It is also interesting that at higher redshifts the hexadecupole which comes purely from velocities (and lensing) is less suppressed w.r.t. the monopole than at low redshift. This is due to the fact that velocities decay less rapidly with increasing redshift than density perturbations which dominate the monopole. The negative quadrupole is even larger than the monopole at $z = 1$ and 2.

From Fig. 2.7 it is also evident that an expansion in multipoles, which is strongly affected by the lensing signal at redshifts $z \gtrsim 1$, is not ideal to extract the lensing signal which is very strongly peaked in the forward direction and contributes similarly to most (even) multipoles.

We have mentioned in the beginning of this section that millions of power spectra $C_\ell(z, z')$ are numerically too costly for parameter estimation via Markov chain Monte Carlo techniques. But when calculating the correlation function via Eq. (2.129), we still need the power spectra and the computational effort is not reduced. In [33] a new method has been introduced which allows a fast direct computation of the correlation function without need of the power spectra. This method has been implemented in a publicly available fast code 'COFFE'[1], see [34] for a description, which allows the computation of the full correlation function in a redshift bin of width $2\Delta z = 0.1$ in about one minute. For a survey with $z \in [0.5, 2.5]$ we would need 20 such correlation functions. For the correlations of different bins of width 0.1 we could then compute the power spectra (integrated over the bin widths). Of course, the covariance matrix for the correlation function is not diagonal and more

[1]The code can be found on `https://github.com/JCGoran/coffe`

difficult to compute than the covariance matrix for angular power spectra, but still, this results in a well manageable computational effort on a small cluster.

2.5 Intensity mapping

Hydrogen is the most abundant element in the Universe, making up about 75% of all baryons. After the recombination of hydrogen, the Universe is neutral until about $z \sim 6 \div 8$ when it gets reionized by UV radiation from the first stars. Neutral hydrogen is denoted by HI in astrophysics while ionized hydrogen or proton gas is denoted HII. After reionization, at $z \lesssim 6$, neutral hydrogen is found mainly in proto-galaxies, i.e. regions where baryons have clustered significantly to allow for cooling and for the recombination of protons and electrons into neutral hydrogen.

A very distinctive line of neutral hydrogen is the 21cm line from the hyperfine transition of aligned proton and electron spins to proton and electron spins with opposite orientation. The proton spin generates a magnetic dipole field to which the electron is subjected. This leads to a contribution to the Hamiltonian of the form

$$\Delta H_{hf} = \frac{\gamma_p e^2}{m_e m_p}\left\{\frac{1}{r^3}\left[3(\mathbf{S}_p\cdot\hat{\mathbf{r}})(\mathbf{S}_e\cdot\hat{\mathbf{r}}) - (\mathbf{S}_p\cdot\mathbf{S}_e)\right] + \frac{8\pi}{3}(\mathbf{S}_p\cdot\mathbf{S}_e)\delta(\mathbf{r})\right\}. \tag{2.137}$$

Here $S_{p,e}$ denotes the (normalized) proton and electron spin vector respectively, $m_{p,e}$ denotes their masses and γ_p is a numerical factor relating the proton spin to its magnetic moment. It is known experimentally to be $\gamma_p = g_p/2 = 2.7928$, we have set $c = \hbar = 1$ as usual. In the ground state of the hydrogen atom, due to spherical symmetry, only the second term contributes. It leads to a splitting between the state with aligned proton and electron spins, $F = 1$ and anti-aligned proton and electron spins, $F = 0$ (F is the total angular momentum of the hydrogen atom) given by

$$E_{10} = 2\frac{8\pi\gamma_p e^2}{3m_e m_p}|\psi(0)|^2 \simeq 5.88\times10^{-6}\text{eV} = h\nu_{10} = hc/\lambda_{10}, \tag{2.138}$$

$$\nu_{10} = 1.420\times10^9 s^{-1}, \qquad \lambda_{10} = 21.10\text{cm}. \tag{2.139}$$

Here ψ is the ground state wave function of the electron (see [35] or any other quantum mechanics book for more details on the hyperfine splitting).

Observing this 21cm line during reionization, $10 > z > 6$, will allow to separate HI and HII regions and to study the evolution and clumpyness of the reionization process. Observing the 21 cm line before or after reionization will allow us to study baryon or matter density fluctuations in a way similar to galaxy number counts. However, instead of counting sources of 21cm emission (or absorption), we can also just measure the intensity of the line coming from different directions without resolving individual sources. This is the 21cm intensity mapping technique which we discuss in this section. Experiments which plan to apply 21cm intensity mapping in the near future are discussed in [36] and, more recently in [37]. Observations at high redshift $z \sim 20$ to 100 would be especially exciting as they open an entirely new window to the early phases of cosmic structure formation before luminous structures form, the so called 'dark ages'.

The HI density is proportional to the neutral hydrogen density, $n_b x_{\rm HI}$, where n_b is the baryon density and $x_{\rm HI}$ is the HI fraction of baryons. If $x_{\rm HI}$ is assumed the be independent of the fluctuation amplitude (which is probably a good approximation before and after the reionization epoch), the HI density fluctuation is given by the baryon density fluctuation,

$$\delta_{\rm HI} = \delta_b \,. \tag{2.140}$$

In order to emit a 21cm photon, the hydrogen atom has to be in the excited state. It is usually excited either by low energy CMB photons, by collisions, or by the 'Wouthuysen–Field effect' which we discuss below.

To derive the first order perturbation equation for HI intensity fluctuations, we consider the brightness I_ν of HI emission of a given cloud of hydrogen. I_ν is the power emitted per Hz, per steradian and per cm^2, it has units of erg/sec/Hz/sr/cm^2. There exists exactly one temperature, called the brightness temperature T_b of I_ν, for which the blackbody spectrum has the intensity I_ν at frequency ν. The brightness temperature, T_b is given in terms of the brightness by

$$I_\nu = \frac{d\rho}{d\nu d\Omega} = \frac{2}{(2\pi)^2}\frac{T_b^3 x^3}{e^x - 1}\,, \tag{2.141}$$

where we have used the standard expression for the energy density of bosons in thermal equilibrium with $N_b = 2$ and $x = p/T_b = 2\pi\nu/T_b$. We set $\hbar = 1$ so that Planck's constant $h = 2\pi$. In the Rayleigh-Jeans limit, $x \ll 1$ which is

most relevant for 21cm photons, we can approximate $e^x - 1 \simeq x$ and obtain

$$I_\nu = 2T_b\nu^2 \quad \text{or} \quad T_b = \frac{I_\nu}{2\nu^2}\,. \tag{2.142}$$

As the brightness scales like $(1+z)^3$ with redshift, this temperature scales as $T_b \propto (1+z)$, like the CMB temperature. The brightness temperature of a hydrogen cloud is

$$T_b = T_S(1 - e^{-\tau_\nu}) + T_R(\nu)e^{-\tau_\nu}\,. \tag{2.143}$$

Here T_S is the spin temperature defined by the ratio of excited hydrogen atoms in the spin 1 state, n_1, and the hydrogen atoms in the ground state with spin 0, n_0 by

$$\frac{n_1}{n_0} = \frac{g_1}{g_0}e^{-E_{10}/T_S}\,, \tag{2.144}$$

where $g_1 = 3$ and $g_0 = 1$ denote the multplicities of the corresponding spin states. $T_R(\nu)$ is the brightness temperature of an external radiation field incident on the cloud (e.g. the CMB) at frequency ν andf τ_ν is the optical depth through the cloud, $\tau_\nu = \int_{\rm cloud}\alpha_\nu d\ell$ where α_ν is the absorption coefficient. In astrophysical applications usually $T_S \gg E_{10}$ so that $n_1 \simeq 3n_0$ and the absorption coefficient must include a correction for stimulated emission. Hence

$$\tau_\nu = \int d\ell\sigma_{01}\left(1 - e^{-E_{10}/T_S}\right)\phi(\nu)n_0 \simeq \sigma_{01}\frac{h\nu}{T_S}(N_{\rm HI}/4)\phi(\nu)\,. \tag{2.145}$$

Here $N_{\rm HI}$ is the column density of neutral hydrogen of the cloud and we used that $n_0 \simeq n_{\rm HI}/4$, and $\phi(\nu)$ is the line profile, $\phi(\nu) = h(1+z)|d\lambda/dz|/L$, where λ is the affine parameter along the photon geodesic, z is the redshift of the line and L is the thickness of the cloud. The cross section σ_{01} for 21 cm absorption is given by

$$\sigma_{01} = \frac{2A_{10}}{8\pi\nu^2}\,, \tag{2.146}$$

where A_{10} is the spontaneous emission coefficient of the 21 cm line. Setting $N_{\rm HI} = Ln_{\rm HI} = Ln_b x_{\rm HI}$ and putting it all together we obtain the following expression for the brightness temperature, see [38]

$$T_b = \frac{3}{32\pi}\frac{h^3 A_{10}}{E_{10}}n_b x_{\rm HI}(1+z)\left|\frac{d\lambda}{dz}\right| \tag{2.147}$$

where again $h = 2\pi$ is Planck's constant. The study of linear perturbations of T_b, assuming that $x_{\rm HI}$ is constant and $n_b \propto \rho$, is presented in detail in [38] . It leads exactly to Eq. (2.118) with $s = 2/5$. Here we do not repeat this derivation as the result is actually not very surprising. For a brightness temperature or an intensity, the reduction of the density by the increased transverse area is exactly compensated by the increase of the number of photons due to focussing. This is a consequence of the photon number conservation which also is the reason that there are no lensing terms in the CMB at first order.

To measure the brightness temperature we can contrast lines of sight through a hydrogen cloud which is irradiated only by the CMB, $T_R = T_{\rm CMB}$, with lines of sight to 'clear CMB'. This yields

$$\begin{aligned} \delta T_b &= T_b - T_0 = \frac{T_S - T_\gamma(z)}{1+z}\left(1 - e^{-\tau_\nu}\right) \simeq \frac{T_S - T_\gamma(z)}{1+z}\tau_\nu \\ &= \left[1 - \frac{T_\gamma(z)}{T_S}\right] \frac{3}{32\pi}\frac{h^3 A_{10}}{E_{21}} n_b x_{\rm HI} \left|\frac{d\lambda}{dz}\right| . \end{aligned} \tag{2.148}$$

This expression is saturated for $T_S \gg T_\gamma$ but is can become arbitrarily negative for small spin temperature, $T_S < T_\gamma$. A negative δT_b just means that we see the line in absorption while for a $T_S > T_\gamma$ we see it in emission. To decide whether we see the 21cm line in emission or absorption, we have to determine the spin temperature T_S.

At early times, $z \geq 200$, the free electrons remaining after recombination keep the baryon fluid in thermal equilibrium with the CMB and we have $T_B = T_\gamma$, where T_B denotes the kinetic baryon temperature. Collisions also keep the spin temperature at this value so that $T_S - T_\gamma = 0$ and we cannot detect the 21cm line. At $z \sim 150$, the heating by Thomson scattering of the remaining electrons drops out of equilibrium, see Ex. 2.5.2. After that time, the baryon temperature decays like $(1+z)^2$ (see e.g. [2]). Initially the spin temperature is in equilibrium with the kinetic baryon temperature dues to collisions, $T_S = T_B$, and we can (in principle) see the 21cm line in absorption at redshifts $150 > z > 30$. However, if there is no additional cooling of the spin temperature, at $z \sim 30$ also collisions drop out of equilibrium and the spin temperature rises back to the CMB temperature so that $\delta T_b \to 0$. However, when first structures form, the so called Wouthuysen–Field effect [39, 40] drives again $T_S \to T_B$. This effect simply takes into account that Lyman-α transitions can change the total spin by 1 or 0. Therefore, Lyman alpha photons can induce a transition from $1_0S_{1/2}$ to $2_1P_{1/2}$ which

can then decay into $1_1S_{1/2}$. and similar with the $1_0S_{1/2}$ to $2_1P_{3/2}$ transition of Hydrogen (Here the first number is n, the principle quantum number, the first index is F, the total angular momentum of the atom, the letter indicates the angular momentum of the electron, S means 0 while P corresponds to 1 and the second index is J, the total angular momentum of the electron.). The Wouthuysen-Field effect couples the hydrogen kinetic temperature and its spin temperature. The latter is expected to always remain somewhat higher than the former, but by how much depends on the model [36].

Recently, the detection of T_b at a redshift centred around $z \simeq 17$ in absorption has been announced by [41]. However, the effect seems to be at least a factor of 2 larger than the most optimistic estimate with $T_S = T_K$. This very difficult experiment, which 'fishes' a ~ -0.5K signal out of a several 1000K background, certainly needs confirmation. The theoretically expected value would have been around -0.1 to -0.2K.

After reionization, at $z \lesssim 6$ inside structures (proto-galaxies and galaxies), the density becomes again large enough so that the kinetic baryon temperature is much higher than the CMB temperature and roughly equal to the spin temperature. In these structures it will be possible to see T_b in emission and its value is independent of the spin temperature, see Eq. (2.148) in the limit $T_S \gg T_\gamma$. To study the angular fluctuations of T_b, we fix a 'clear CMB' direction and simply study

$$\Delta T_b = \delta T_b(\mathbf{n}) - \delta T_b(\mathbf{n}') = \delta\bar{T}_b[\Delta_T(\mathbf{n}) - \Delta_T(\mathbf{n}')] \tag{2.149}$$

like for the CMB, see [2]. In this expression, the somewhat ill defined 'clear CMB' direction drops out and we may use (2.148) in the limit $T_S \gg T_\gamma$. At low redshift, $z \lesssim 6$, we therefore expect fluctuations of the brightness temperature given by Eq. (2.118) with $s = 2/5$ and its own bias $b(z)$ and evolution bias $b_e(z)$.

Summarizing, we have found that the 21cm emission line is interesting for at least three different reasons

1. It can pave a way to observe the baryon density and its fluctuation at $150 > z > 50$ when there are not yet any structures emitting photons in the Universe, the so called dark ages.

2. It is sensitive to the neutral hydrogen fraction $x_{\rm HI}$ which has fluctuations of order unity during reionisation. These, in principle allow us to study in detail the process of reionization at redshift $10 > z > 6$.

3. At lower redshifts, $z \lesssim 6$, neutral hydrogen is predominantly in structures where also the spin temperature is much higher than the CMB temperature. At these redshifts we can detect 21 cm radiation in emission and we expect it to be a very useful additional trace of large scale structure.

Since the frequency of the 21cm is so well defined, all these observations have exquisite redshift resolution.

Of course, the 21cm line is not the only line which can be observed. It may also be interesting to study other hydrogen lines, e.g. the Lyman-α lines or lines of heavier elements like carbon which are generated in cosmic structures, see [37] for a recent review where preliminary detections of a rotational carbon-monoxide (CO) line, a CII fine-structure, Lyman-α and H_α lines as well as low redshift 21cm measurements are described. So far these detections have been made by correlating intensity mapping measurements with galaxy surveys, but clearly this is just the beginning...

2.5.1 Exercise

From the power spectrum to the correlation function
Consider a power spectrum which depends not only on k but also on its direction cosine w.r.t. a fixed direction $\mathbf{n}$. Expanding this dependence in Legendre polynomials,

$$P(k,\mu) = \sum_n P_n(k) L_n(\mu)\,, \qquad \mu = \mathbf{n}\cdot\mathbf{k}/k\,, \tag{2.150}$$

show that the correlation function is given by

$$\xi(r,\mu) = \sum_n (i)^n \xi_n(r) L_n(\mu)\,, \qquad \mu = \mathbf{n}\cdot\mathbf{r}/r\,, \tag{2.151}$$

where

$$\xi_n(r) = \int \frac{dk k^2}{2\pi^2} P_n(k) j_n(kr)\,. \tag{2.152}$$

Hint: Use the addition theorem of spherical harmonics.

Therefore, if both, the correlation function and the power spectrum are real, only even powers of μ are possible.

2.5.2 Exercice

Decoupling of the baryon temperature from the CMB
Using the following expression for the fraction of ionized electrons after recombination,

$$x_R = 1.2\times 10^{-5}\Omega_m^{1/2}/(\Omega_B h)\,,$$

show that heating by Thomson scattering of these electrons with CMB photons drops out of thermal equilibrium at $z_\gamma \simeq 150$. For this, use that the Thomson cooling (heating) rate is

$$\Gamma = \frac{x_R}{t_\gamma} \qquad \text{with} \quad t_\gamma = \frac{m_e}{8\sigma_T \rho_\gamma}\,. \tag{2.153}$$

Bibliography

[1] **Planck** Collaboration, N. Aghanim *et al.*, "Planck 2018 results. VI. Cosmological parameters," arXiv:1807.06209 [astro-ph.CO].

[2] R. Durrer, *The Cosmic Microwave Background*. Cambridge University Press, 2008.

[3] R. K. Sachs and A. M. Wolfe, "Perturbations of a cosmological model and angular variations of the microwave background," *Astrophys. J.* **147** (1967) 73–90. [Gen. Rel. Grav.39,1929(2007)].

[4] G. Arfken and H. Weber, *Mathematical Methods for Physicists*. Harcourt Academic Press, New York, 1966.

[5] M. Abramowitz and I. Stegun, *Handbook of Mathematical Functions*. Dover Publications, New York, 9th printing ed., 1970.

[6] **COBE** Collaboration, G. F. Smoot *et al.*, "Structure in the COBE differential microwave radiometer first year maps," *Astrophys. J.* **396** (1992) L1–L5.

[7] A. Lewis, A. Challinor, and A. Lasenby, "Efficient computation of CMB anisotropies in closed FRW models," *Astrophys. J.* **538** (2000) 473–476, arXiv:astro-ph/9911177 [astro-ph].

[8] J. Lesgourgues, "The Cosmic Linear Anisotropy Solving System (CLASS) I: Overview," arXiv:1104.2932 [astro-ph.IM].

[9] D. Blas, J. Lesgourgues, and T. Tram, "The Cosmic Linear Anisotropy Solving System (CLASS) II: Approximation schemes," *JCAP* **1107** (2011) 034, arXiv:1104.2933 [astro-ph.CO].

[10] J. Silk, "Cosmic black body radiation and galaxy formation," *Astrophys. J.* **151** (1968) 459–471.

[11] **DES** Collaboration, M. A. Troxel *et al.*, "Dark Energy Survey Year 1 results: Cosmological constraints from cosmic shear," *Phys. Rev.* **D98** no. 4, (2018) 043528, arXiv:1708.01538 [astro-ph.CO].

[12] S. Joudaki *et al.*, "KiDS-450 + 2dFLenS: Cosmological parameter constraints from weak gravitational lensing tomography and overlapping redshift-space galaxy clustering," *Mon. Not. Roy. Astron. Soc.* **474** no. 4, (2018) 4894–4924, arXiv:1707.06627 [astro-ph.CO].

[13] B. Ghosh, R. Durrer, and E. Sellentin, "General Relativistic corrections in density-shear correlations," *JCAP* **1806** no. 06, (2018) 008, arXiv:1801.02518 [astro-ph.CO].

[14] D. N. Limber, "The Analysis of Counts of the Extragalactic Nebulae in Terms of a Fluctuating Density Field. II," *Astrophys. J.* **119** (1954) 655.

[15] M. LoVerde and N. Afshordi, "Extended Limber Approximation," *Phys. Rev.* **D78** (2008) 123506, arXiv:0809.5112 [astro-ph].

[16] C. Bonvin, R. Durrer, and M. A. Gasparini, "Fluctuations of the luminosity distance," *Phys. Rev.* **D73** (2006) 023523, arXiv:astro-ph/0511183 [astro-ph]. [Erratum: Phys. Rev.D85,029901(2012)].

[17] P. Schneider, J. Ehlers, and E. Falco, *Gravitational lenses*. Springer-Verlag, Berlin, 1993.

[18] M. Sasaki, "The Magnitude - Redshift relation in a perturbed Friedmann universe," *Mon. Not. Roy. Astron. Soc.* **228** (1987) 653–669.

[19] P. J. Peebles, *The Large Scale Structure of the Universe*. Princeton University Press, 1980.

[20] N. Kaiser, "Clustering in real space and in redshift space," *M.N.R.A.S.* **227** (July, 1987) 1–21.

[21] C. Alcock and B. Paczynski, "An evolution free test for non-zero cosmological constant," *Nature* **281** (1979) 358–359.

[22] F. Montanari and R. Durrer, "A new method for the Alcock-Paczynski test," *Phys. Rev.* **D86** (2012) 063503, arXiv:1206.3545 [astro-ph.CO].

[23] F. Lepori, E. Di Dio, M. Viel, C. Baccigalupi, and R. Durrer, "The Alcock Paczyski test with Baryon Acoustic Oscillations: systematic effects for future surveys," *JCAP* **1702** no. 02, (2017) 020, arXiv:1606.03114 [astro-ph.CO].

[24] N. Dalal, O. Dore, D. Huterer, and A. Shirokov, "The imprints of primordial non-gaussianities on large-scale structure: scale dependent bias and abundance of virialized objects," *Phys. Rev.* **D77** (2008) 123514, arXiv:0710.4560 [astro-ph].

[25] E. Di Dio, F. Montanari, A. Raccanelli, R. Durrer, M. Kamionkowski, and J. Lesgourgues, "Curvature constraints from Large Scale Structure," *JCAP* **1606** no. 06, (2016) 013, arXiv:1603.09073 [astro-ph.CO].

[26] C. Bonvin and R. Durrer, "What galaxy surveys really measure," *Phys. Rev.* **D84** (2011) 063505, arXiv:1105.5280 [astro-ph.CO].

[27] A. Challinor and A. Lewis, "The linear power spectrum of observed source number counts," *Phys.Rev.* **D84** (2011) 043516, arXiv:1105.5292 [astro-ph.CO].

[28] F. Montanari and R. Durrer, "Measuring the lensing potential with tomographic galaxy number counts," *JCAP* **1510** no. 10, (2015) 070, arXiv:1506.01369 [astro-ph.CO].

[29] D. Alonso and P. G. Ferreira, "Constraining ultralarge-scale cosmology with multiple tracers in optical and radio surveys," *Phys. Rev.* **D92** no. 6, (2015) 063525, arXiv:1507.03550 [astro-ph.CO].

[30] V. Iršič, E. Di Dio, and M. Viel, "Relativistic effects in Lyman- forest," *JCAP* **1602** no. 02, (2016) 051, arXiv:1510.03436 [astro-ph.CO].

[31] R. Durrer and V. Tansella, "Vector perturbations of galaxy number counts," *JCAP* **1607** no. 07, (2016) 037, arXiv:1605.05974 [astro-ph.CO].

[32] E. Di Dio, F. Montanari, J. Lesgourgues, and R. Durrer, "The CLASSgal code for Relativistic Cosmological Large Scale Structure," *JCAP* **1311** (2013) 044, arXiv:1307.1459 [astro-ph.CO].

[33] V. Tansella, C. Bonvin, R. Durrer, B. Ghosh, and E. Sellentin, "The full-sky relativistic correlation function and power spectrum of galaxy number counts: I. Theoretical aspects," arXiv:1708.00492 [astro-ph.CO].

[34] V. Tansella, G. Jelic-Cizmek, C. Bonvin, and R. Durrer, "COFFE: a code for the full-sky relativistic galaxy correlation function," *JCAP* **1810** no. 10, (2018) 032, arXiv:1806.11090 [astro-ph.CO].

[35] D. Park, *Introduction to the Quantum Theory*. Springer-Verlag, Berlin, 1974.

[36] S. Furlanetto, S. P. Oh, and F. Briggs, "Cosmology at Low Frequencies: The 21 cm Transition and the High-Redshift Universe," *Phys. Rept.* **433** (2006) 181–301, arXiv:astro-ph/0608032 [astro-ph].

[37] E. D. Kovetz *et al.*, "Line-Intensity Mapping: 2017 Status Report," arXiv:1709.09066 [astro-ph.CO].

[38] A. Hall, C. Bonvin, and A. Challinor, "Testing General Relativity with 21-cm intensity mapping," *Phys. Rev.* **D87** no. 6, (2013) 064026, arXiv:1212.0728 [astro-ph.CO].

[39] S. A. Wouthuysen, "On the excitation mechanism of the 21-cm (radio-frequency) interstellar hydrogen emission line.," *Astron. J.* **57** (Jan, 1952) 31–32.

[40] G. B. Field, "The Spin Temperature of Intergalactic Neutral Hydrogen.," *Astrophys. J.* **129** (May, 1959) 536.

[41] J. D. Bowman, A. E. E. Rogers, R. A. Monsalve, T. J. Mozdzen, and N. Mahesh, "An absorption profile centred at 78 megahertz in the sky-averaged spectrum," *Nature* **555** no. 7694, (2018) 67–70, arXiv:1810.05912 [astro-ph.CO].